Universidade de Aveiro
2022

Patrícia Alexandra Carvalho Santos Graça

MODELAÇÃO E CARACTERIZAÇÃO TÉRMICA DE MATERIAIS DE MUDANÇA DE FASE PARA SOLUÇÕES DE AQUECIMENTO AMBIENTE

MODELLING AND THERMAL CHARACTERIZATION OF PHASE CHANGE MATERIALS FOR HEATING BUILDING SOLUTIONS

Universidade de Aveiro
2022

Patrícia Alexandra Carvalho Santos Graça

MODELAÇÃO E CARACTERIZAÇÃO TÉRMICA DE MATERIAIS DE MUDANÇA DE FASE PARA SOLUÇÕES DE AQUECIMENTO AMBIENTE

MODELLING AND THERMAL CHARACTERIZATION OF PHASE CHANGE MATERIALS FOR HEATING BUILDING SOLUTIONS

Dissertação apresentada à Universidade de Aveiro para cumprimento dos requisitos necessários à obtenção do grau de Mestrado em Engenharia Mecânica, realizada sob orientação científica de Tiago Manuel Rodrigues da Silva, Investigador Doutorado (nível 1) do Departamento de Engenharia Mecânica da Universidade de Aveiro, e de Mónica Sandra Abrantes de Oliveira Correia, Professora Associada c/ Agregação da Universidade de Aveiro.

Esta dissertação teve o apoio dos projetos UIDB/00481/2020 e UIDP/00481/2020 - Fundação para a Ciência e a Tecnologia; e CENTRO-01-0145 FEDER-022083 - Programa Operacional Regional do Centro (Centro2020), através do Portugal 2020 e do Fundo Europeu de Desenvolvimento Regional.

O júri / The jury

Presidente / President	**Prof. Doutor Fernando José Neto da Silva** Professor Auxiliar da Universidade de Aveiro
Vogais / Committee	**Doutor Tiago Manuel Rodrigues da Silva** Investigador Doutorado (nível 1) da Universidade de Aveiro
	Doutor António José Pereira de Figueiredo Investigador Doutorado (nível 1) da Universidade de Aveiro

Agradecimentos / Acknowledgements

To this academy, for so much it has taught me beyond technical knowledge. For having both sharpen and polished the personal growth, team spirit and ingenuity that allowed me to begin a career I have been dreaming with since I was a little girl. To the professors and colleagues, throughout all my school years, who inspired and motivated me to not underestimate myself.

To my friends who encouraged me to stay curious and to pursue my ideas, regardless of how crazy and unreachable they might have appeared at times. For joining me on this wild and memorable journey that was college. For all the amazing memories that we shared and the friendship that will remain for a lifetime.

To my parents, for the tough love that shaped me and turned me into who I am today. For all the sacrifices made to provide me with the opportunities I was lucky to have. For always believing in me even when I almost stopped believeing in myself.

Specially, to a little girl that many years ago asked the stars, how big was the universe and how small was the atom, how fast was a rocket and how did bridges stood still. I want to thank her for staying up all those nights daydreaming about the cosmos and the meaning of life. For wanting to know where energy comes from and how only the planes and the birds do not fall from the skies. I want to thank her for asking all the questions she could think of, for never having lost neither the need to wonder around in thoughts or the will to study, to understand the answers to some of those questions today.

"Scientists study the world as it is,
Engineers create the world that never has been."
-Theodore von Kármán

Palavras-chave Materiais de Mudança de Fase; Armazenamento de Energia; Análise Numérica; Calor Latente; Eficiência Energética; Estudo Paramétrico

Resumo

Os sistemas de armazenamento de energia podem fazer uma grande diferença para reduzir o custo e a necessidade do consumo de combustíveis fósseis, seja mudando o tempo de absorção de energia para fora do pico de procura, ou sendo acoplados a métodos de captura de energia e consequentemente armazenando energia de alternativas verdes.

Este trabalho apresenta um estudo paramétrico de forma de uma solução de aquecimento de edifícios residenciais que recorre a materiais de mudança de fase como sistema de armazenamento de energia térmica num permutador de calor. Uma explicação teórica dos princípios de armazenamento de energia destes materiais é apresentada, seguido por um estado de arte das aplicações atuais desta tecnologia em soluções de construção. Um modelo é então desenvolvido com base numa solução investigada de um ácido láurico e a melhoria da performance da sua aplicação é avaliada com recurso ao Ansys Fluent®. A calibração e validação do mesmo é realizada em relação aos resultados presentes no referido artigo.

O impacto da forma das superfícies de transferência de calor nos fluxos de convecção induzidos é estudado em 4 casos com os respectivos alcances horizontal incrementalmente mais elevados. Os resultados revelaram que para cada aumento de 5 mm no eixo horizontal da superfície de transferência de calor, verifica-se uma média de 9% de diminuição no tempo de carregamento do PCM, consequência de um aumento de 5% na taxa de fusão do material. O perímetro mais elevado em cada incremento de 5 mm também fornece um aumento considerável de 20% no valor de pico da taxa de transferência de calor, bem como um tempo de carregamento de 7% economizado para atingir os valores máximos da velocidade dos fluxos convectivos induzidos. O estudo optimizado proposto que apresenta melhores resultados mostra uma redução no tempo de carregamento de 38% quando comparado ao estudo inicial.

Keywords Phase Change Material; Energy Storage; Numerical Analysis; Latent Heat; Energy Efficiency; Parametric Study

Abstract

Energy storage systems can make a big difference to reduce both the cost and the impact of fossil fuel's consumption, by either shifting the charging time to off peak-load of demand or being coupled and store energy from green alternatives to energy capture methods.

This work presents a shape parametric study on a home heating solution that resorts to a shell and tube heat exchanger system with Phase Change Materials as the Thermal Energy Storage method. A theoretical explanation of its energy storage principles is presented, followed by a state of the arts description of the current applications of this technology in household construction features. A model is then developed based on a researched solution with lauric acid and the efficiency enhancement of its application is performed using Ansys Fluent®. Its calibration and validation is consummated against the results of the already exiting article.

The impact of the shape of the heat transfer surface in the convection flows is adressed resorting to parametric studies of 4 cases with their respective horizontal reach incrementally higher. Results revealed that for each 5 mm increase in the heat transfer surface horizontal axis, an average of a 9% decrease in the PCM charging time, resultant of a 5% increase in the melting rate of the material. The higher perimeter for each 5 mm increment also provides a considerable boost of 20% in the peak value of heat transfer rate, as well as a 7% charging time saved to reach the induced convection velocity roof values. The most optimized study of the proposed cases presented a charging time 38% faster than the original.

Contents

List of Tables

List of Figures

Symbols

β	Thermal Energy Coefficient
c_p	Specific Heat Capacity
g	Gravity
H	Entalpy
k	Thermal Conductivity
L	Latent Heat
λ	Liquid Fraction
m	Mass
n	Total Number of Terms
p	Pressure
Q_{latent}	Latent Heat
$Q_{sensible}$	Sensible Heat
ρ	Density
ρ_v	Dinamic Viscosity
S	Mushy Zone Parameter
T	Temperature
T_{pc}	Phase Change Temperature
θ	Element Angle
v	Fluid Velocity
y_a	Average Reference Result
y_o	Obtained Result
y_r	Reference Result

Acronyms

CAD Computer-Aided Design , 26

CFD Computational Fluid Dynamics , 25

CVRMSE Coefficient of Variation of the Root Mean Square Error , 36, 37

DSC Differential Scanning Calorimetry , 8

FTIR Fourier Transform Infrared Spectroscopy , 8

GOF Goodness of Fit , 36, 37

HTF Heat Transfer Fluid , 25, 27, 32, 40, 42, 58

HTS Heat Transfer Surface , 4, 26, 27, 33, 40–42, 44, 46, 47, 49, 52–55, 58, 59

IGS Initial Graphics Exchange , 26

NMBE Normalized Mean Bias Error , 36, 37

PCM Phase Change Materials , 1, 3, 4, 7–27, 32, 33, 35, 37–41, 45–49, 52–55, 58, 59

SS-PCM Shape-Stabilized Phase Change Materials , 20, 21

STHE Shell and Tube Heat Exchanger , 25, 26, 41, 58

TES Thermal Energy Storage , 1, 5, 15, 20

TGA Thermogravimetric Analysis , 8

ZERB Zero Energy Consumption Residential Building , 24

Chapter 1

Introduction

1.1 Motivation

In the last decades, society has been exposed every day to news channels and newspapers delivering reports on energy status with increasing concern. That is because society's dependency on immediate energy availability keeps increasing, and so, energy has become one of civilization's news daily topic.

However, it was not until the middle of the 19^{th} century, with the industrial revolution, that the demand of energy really started to make a relevant impact, as observable in Figure 1.1. Even though energy has always been around, only by then its usages were massively required and consequently put into practice. Mainly since this period, and because it aligned with an incredible technology development era, the research of energy properties, sources and applications began and kept evolving at a fast pace.

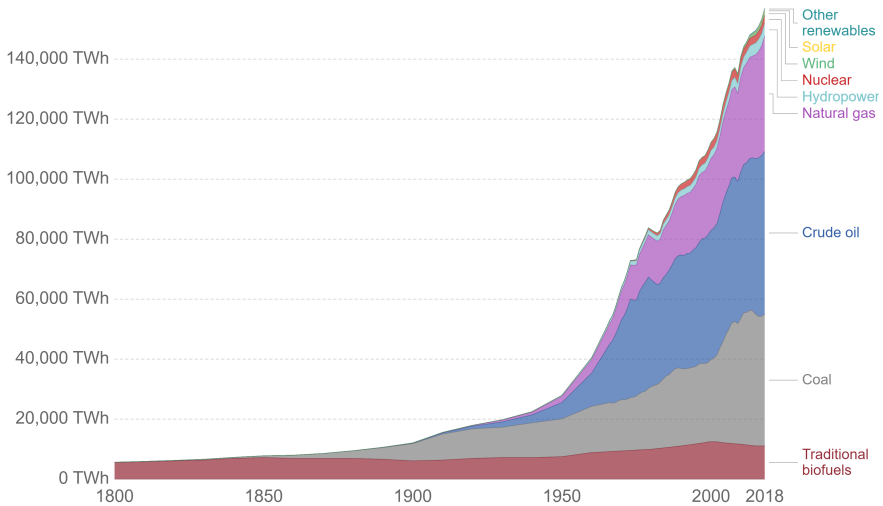

Figure 1.1: Global primary energy consumption evolution [1]

Analyzing energy employment at a global scale, as displayed in Figure 1.2, the four main sectors of energy consumption are: i) the transport systems; ii) the industries; iii) the supply to households and last; iv) the sector of services to the community [2].

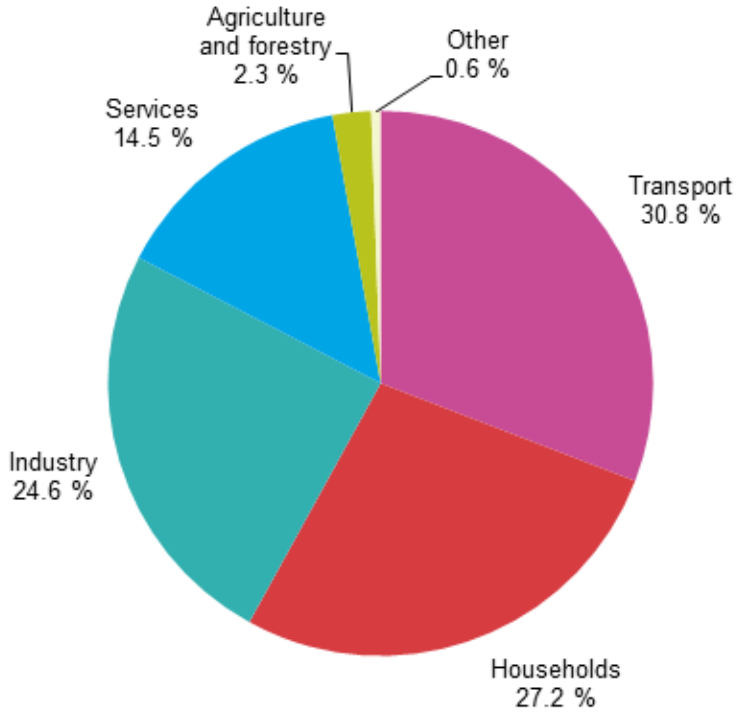

Figure 1.2: Final energy consumption by sector [2]

As a consequence of this excessive energy consumption, growing need and startled by increasing concerns of environmental nature, bigger investments have been made worldwide, as we can observe in Figure 1.3. The investments on this valuable resource, have focused on finding, as well as optimizing, new methods and techniques for its:

1. capture;
2. transformation;
3. distribution;
4. storage;
5. employment;

More efficient procedures have been studied, developed and implemented to capture energy from clean and renewable sources. Nevertheless, focusing the research on capturing more green energy without being able to take full advantage of it at its highest performance may not be the most efficient path. So, other options that do not substitute, but do in fact complement, the previously achieved progress, can be considered.

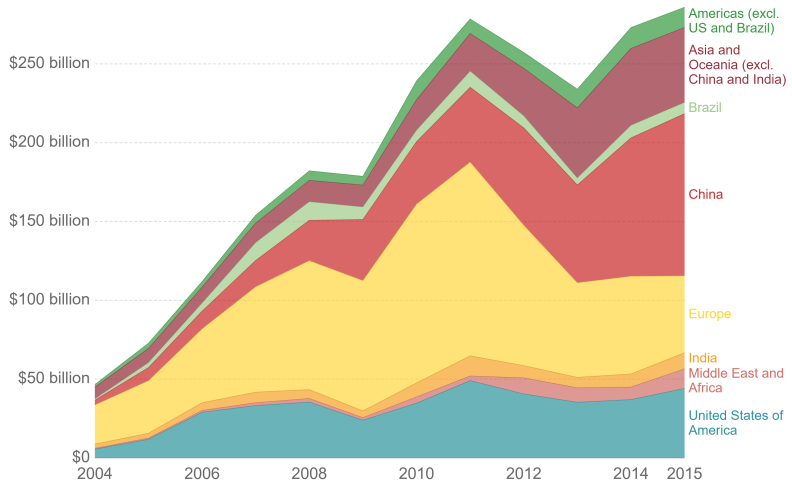

Figure 1.3: Renewable energy investment [1]

The most pressing goal at a daily life point of view, is to guarantee that the regular citizen, as well as industries, can be sure of its availability at any time, as quickly and effortlessly as possible and under the best feasible circumstances. However, because most green energy sources are dynamic and in some cases unpredictable, like the solar exposure or the uncertainty of the wind speed, energy storage becomes a crucial topic.

My motivation is to present an environmentally friendly energy storage solution, to assist green energy capture methods. That way, when possible, the conventional energy sources that would be required, can be replaced by the energy previously stored. Considering the trajectory that global energy consumption rate has had so far, and given that this values are only expected to increase, the impact of widely implementing such systems in the future, is very significant to both the health of the planet as well as the consumer's wallets.

1.2 Objectives

The aim of this thesis is to propose a parametric analysis of a currently documented solution, and study the possibility of increasing its efficiency by adjusting the values of pertinent variables. This way attempting to increase the efficiency of energy storage procedures in applications related with providing thermal comfort.

To achieve this, Phase Change Materials will be incorporate into one building feature and used as a mean to store energy. Absorbing it when it is convenient and abundant, releasing it when required for home heating purposes.

1.3 Structure Outline

Chapter 1 This chapter presents not only the reasons why I believe this thesis topic has a significant impact, also my motivations behind its selection, as well as the goals that were set to achieve. This chapter also presents an overall outline of the stages of development of this thesis.

Chapter 2 In this chapter, an analysis of the theory behind the energetic processes that allow for storage was intended. Also presents the type of materials able to store great amounts of energy, Phase Change Materials, their main characteristics, properties and classification.

Chapter 3 After understanding the theory behind the materials in study in chapter 2, a state of the art of their applications focusing on building features is presented. Given the extended range of these solutions, one specific is chosen to investigate at length. Floor applications are investigated in greater detail to analyse possible strategies to follow.

Chapter 4 This chapter describes the article chosen from the floor applications' research process. Its solution and respective numerical definitions are used to build a numerical model which is explained in detail. The results obtained are compared with the original article's in order to achieve validation. Once the model is validated, a strategy to present a parametric study in the following chapter is outlined.

Chapter 5 Based on the strategy defined, a parametric study of the previous solution evaluates the influence of the HTS horizontality in a variety of different thermal aspects of the solution. Variables such as i) melting rate, ii) total melting time, iii) heat transfer and iv) PCM convection's velocity. The numerical definitions used are presented, as well as the adopted changes in the HTS geometries. Still in this chapter, the results obtained are treated, analysed and discussed.

Chapter 6 Starts by revisiting the goals set inittialy, and after analising the results obtained, evaluating whether or not they were achieved. Presents not only the takeaways of the results discussion, but also the limitations experienced during the development process, as well as the lessons learned from the analysis conducted.

Chapter 2

Theory Analysis

2.1 Energy Storage

There are a few conventional approaches when it comes to energy storage. The most regular ones involve i) kinetic or ii) potential energy, like inertia wheels and dams. Other approach is iii) chemical energy, applied in the everyday batteries, also iv) electric energy based solution as in capacitors or, more recently, v) superconducting magnetic energy storages, and last but not least, vi) thermal energy [3].

If a mass is receiving a certain amount of thermal energy from a heat transfer process, it may be either from a chemical source, like the heat of a reversible exothermical chemical reaction, or from a physical process. When the source of this energy absorption is through physical processes, it might be being stored as sensible or latent heat, depending on the amount of energy previously contained by the mass in question [4]. Figure 2.1 shows the durability, commercial viability, temperature range and storage density analysis of each of the previous processes.

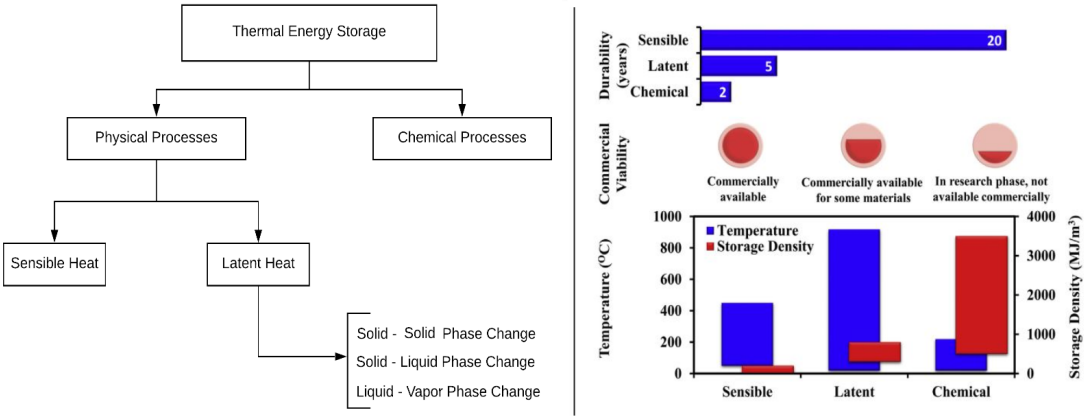

Figure 2.1: Left: Thermal energy storage; Right: Durability, commercial viability, temperature range and storage density for each type of TES [5]

To differentiate sensible from latent heat, an analysis on the mass internal energy during absorption is required.

2.1.1 Sensible Heat Storage

If the amount of energy previously stored was so, that the transfer has no interference in the physical state of the mass but its temperature rises with the increase of energy, then the energy provided is being stored as sensible heat. According to the equation 2.1, the ratio between the amount of energy stored ($Q_{sensible}$) and the temperature difference registered in the mass ($T_f - T_i$), is the result of a property of the material called heat capacity (c_p).

$$Q_{sensible} = \int_{T_i}^{T_f} m\ c_p\ dT\ [J] \tag{2.1}$$

Sensible heat is the most used process to store thermal energy. A few of the concerns when analysing this process as a storage mean, is the fact that the amount of energy that can be stored depends on what temperature difference between the heat sources can be achieved.

2.1.2 Latent Heat Storage

The energy absorbed or released by a mass in a phase change is referred to as latent heat. The main advantage of this type of heat storage, is the amount of energy that can be stored with a considerably small temperature variation since the energy stored in the mass depends only on the enthalpic variation associated with the phase change, which occurs at a constant temperature, T_{pc} .

$$Q_{latent} = \Delta H = m\Delta h = \int_{h_i}^{h_f} m\ dh\ [J] \tag{2.2}$$

Even though, any of the changes from one phase to another is suitable for storing or releasing latent energy, the solid-liquid happens to be, more often, the most favorable. Due to the little volume variation and high storage capacity, which most materials do not present at a liquid-vapor transition stage.

2.1.3 Overall Heat Storage

As shows Figure 2.2, when a mass receives energy, the amount it stores depends on the difference between the initial temperature (T_1) and the final temperature (T_2). In case of a phase change temperature (T_{pc}) being reached in the process, also the amount of energy required for the phase change is stored.

$$Q_{stored} = m \times \left[\int_{T_1}^{T_{pc}} c_{p,s}\ dT + \Delta h + \int_{T_{pc}}^{T_2} c_{p,l}\ dT \right]\ [J] \tag{2.3}$$

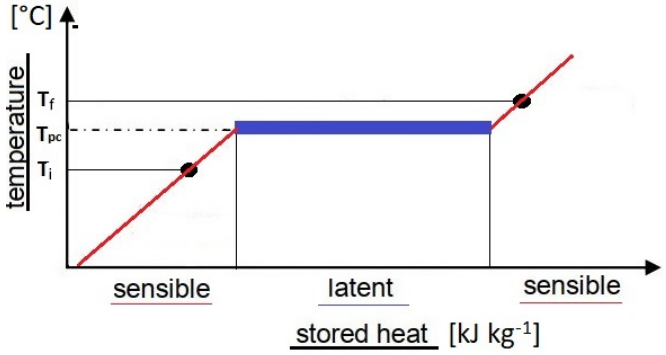

Figure 2.2: Energy storage with temperature variation

2.2 Phase Change Materials

2.2.1 Properties

Follows an analysis of the properties that make these materials special enough to possibly have a major impact in the efficiency of energy management. To be considered a PCM, the material's behaviour and phase change properties must be adequate and of use for later applications. In order to store as much energy as possible, the material must have:

1. Adequate phase change temperature so that the energy can be absorbed as latent heat instead of sensible;
2. High storage capacity per unit of mass, so that the energy stored can be maximized for the same volume of material;
3. High storage efficiency, meaning low thermal inertia also referred to as high conductivity for fast transfers;
4. Little variation of volume with phase change to optimize the space of the solution application;
5. Kinetically, in order to avoid subcooling, the crystallization speed must be relatively high. Subcooling effect is when latent heat is not released as soon as the solidificatioin temperature is reached, instead, the temperature of the material will gradually decrease until such a point where crystallisation begins.
6. The charge/discharge process must be totally reversible and its cycle number elevated to ensure an appropriate lifetime;
7. Economically, to be able to compete with the already available solutions, the cost of acquisition and maintenance should be as low as possible;

2.2.2 Characterization Techniques

There are different methods and techniques, to characterize these materials as to their chemical and thermal properties.

In order to determine melting temperatures, latent heat of fusion and specific heat capacities of the materials Differential Scanning Calorimetry (DSC) is performed [6].

On the other hand, if the thermal conductivity of a material needs to be determined then T-history method is the go to process [6].

Thermogravimetric Analysis (TGA) is used for thermal stability and thermal reliability and Fourier Transform Infrared Spectroscopy (FTIR) for chemical structure and stability [5].

2.2.3 Classification

After analysing the properties required from a material to be considered a PCM, those materials can be classified according to their chemical composition in three main classes, i) organic, ii) inorganic and iii) eutetic and in subclasses as presented in Figure 2.3

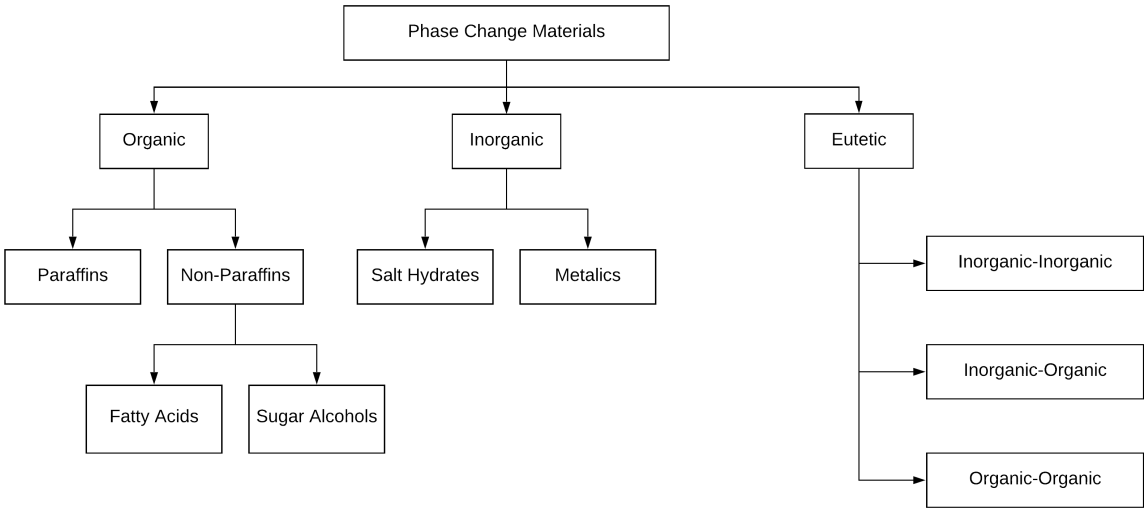

Figure 2.3: Types of PCM [6]

Organics

The Organic Phase Change Materials present characteristics like high melting latent heat and low or intermediate melting temperatures, which are directly dependent on how big the molecules are. Their thermal behaviour is relatively stable and lastly, no subcooling phenomenon occurs.

However, these materials are inflammable, have a lot of thermal inertia, vary a lot in volume during phase change (around 10%), and its phase change may occur in a higher temperature interval, rather than in an accurate melting temperature.

Paraffin based This is the most common type of organic PCM. Its molecule contains hydrogen and carbon atoms with a chemical formula that respects C_nH_{2n+2}.
The melting temperature for each chemical compound increases with the number of atoms in its chemical formula.

Table 2.1: Paraffin based PCM examples [7]

PCM	***Nº Carbon Atoms***	***Melting Temp.,*** T_{pc} ***[ºC]***	***Melting Enthalpy,*** Δh ***[kJ/kg]***
$C_{14}H_{30}$	*14*	*6*	*230*
$C_{18}H_{38}$	*18*	*28.2*	*244*
$C_{20}H_{42}$	*20*	*36.1*	*247*
$C_{21}H_{44}$	*21*	*40.5*	*213*

Fatty Acids These compounds are composed by molecules, that unlike paraffins, contain oxygen atoms in its composition. The biggest concern with these types of PCM is its slightly lower energy storage capacity and the possibility of causing corrosion in some materials.

Table 2.2: Fatty acids PCM examples [7]

PCM	***Nº Carbon Atoms***	***Melting Temp.,*** T_{pc} ***[ºC]***	***Melting Enthalpy,*** Δh ***[kJ/kg]***
$CH_3(CH_2)_6COOH$	*8*	*16*	*149*
$CH_3(CH_2)_{10}COOH$	*12*	*42-44*	*178*
$CH_3(CH_2)_{14}COOH$	*16*	*61*	*185*

Sugar Alcohols This class of organic materials has been studied more recently. They have high storage capacity. However these compounds present us with some level of subcooling which is not favourable for regular applications.

Table 2.3: Sugar alchols PCM examples [7]

PCM	***Melting Temp.,*** T_{pc} ***[ºC]***	***Melting Enthalpy,*** Δh ***[kJ/kg]***
$C_5H_7(OH)_5$	*94*	*263*
$C_4H_6(OH)_4$	*120*	*340*
$C_6H_8(OH)_6$	*188*	*351*

Inorganics

Originally this type of PCM was the most used due to its general low cost and high capacity storage. It can be divided into two main classes, *Hydrated Salts* and *Metalics*.

Salt Hydrates These compounds are a mixture of at least 2 elements, water and a salt, at a variable proportion.

Among other properties, these PCM are chemically stable and safe, though highly corrosive. The fact that it contains various elements leads to different phase change temperatures within the same material which causes instability in the phase change process. Also, these materials present the most subcooling phenomenon of the inorganic category.

This class of PCM was the first kind of PCM to be explored mainly due to its low cost.

Table 2.4: Salt hydrates PCM examples [7]

PCM	***Melting Temp.,*** T_{pc} ***[ºC]***	***Melting Enthalpy,*** Δ_h ***[kJ/kg]***
$LiClO_3 + 3H_2O$	*8*	*155*
$Na_2HPO_4 + 12H_2O$	*34-44*	*280*
$Ba(OH)_2 + H_2O$	*117*	*165*
$LiNO_3$	*254*	*360*
$MgCl_2$	*714*	*452*

Eutetic

By combining either organic, inorganic or both, we can vary the material's properties and develop a new type of PCM. By being able to adjust these compounds, it's possible to specify phase change parameters to use in real applications.

The ability to blend two or more components is highly beneficial in terms of thermal properties enhancement to specific requirements of certain applications. These materials are the most expensive ones comparing to the other types.

Table 2.5: Eutetic PCM examples [7]

PCM	***Melting Temp.,*** T_{pc} ***[ºC]***	***Melting Enthalpy,*** Δ_h ***[kJ/kg]***
$C_{14}H_{28}O_2 + C_{10}H_{20}O_2$	*24*	*147.7*
$CaCl_2 + MgCl_2.H_2O$	*25*	*95*
$CH_3ONH_2 + NH_2CONH_2$	*27*	*163*
$Ca(NO)_3.4H_2O + Mg(NO)_3.6H_2O$	*30*	*136*

2.2.4 Comparison

Knowing now, which types are available, we can analyse advantages and disadvantages of each option. In this next Table 2.6 a summed up list of advantages and disadvantages is presented for each type.

Table 2.6: Summary of the advantages and disadvantages of each type of PCM [5]

Type	Advantages	Disadvantages
Organic	Freeze without much super-cooling or sub-cooling Ability to be incorporated directly Low vapor pressure in phase change process Good thermal performance Ability to melt congruently Self-nucleating properties Compatibility with conventional material of construction Availability in large temperature range No segregation Chemically stable High heat of fusion Safe and non-reactive Recyclable	Low thermal conductivity in their solid state. Some are insoluble in water Burn easily Low phase change enthalpy Low density Require large surface area High heat transfer rates are required during the freezing cycle. Volumetric latent heat storage capacity is low Flammable. This can be easily alleviated by a proper container More expensive High volumetric expansion Low heat capacity
Inorganic	High thermal conductivity Large heat storage capacity Lower volumetric expansion High heat of fusion per unit volume Less costly Non-flammable Sharp phase-change Greater phase change enthalpy Recyclable	High degree of supercooling Lack of thermal stability Phase segregation Incongruent melting and dehydration during thermal cycling Some have high weight Corrosive Prone to degradation Chemical instability Compatibility issues with some building materials Requires container and support
Eutectics	Sharp melting temperature High volumetric thermal storage density No phase segregation and congruent phase change	Lack of currently available test data of thermo-physical properties Low total latent heat capacity Some of eutectics suffer from super-cooling effect Strong Odor Costly

2.2.5 Incorporation Types

The PCM can be encapsulated. The two main reasons for that, is to pack the liquid-phase of the PCM, and to prevent any leakage. Leaks can be harmful to the environment or change the composition of the PCM.

The encapsulation process carries the benefit of possibly acting as a construction element, meaning its incorporation may add mechanical stability to some applications. This type of integration of PCM can be categorized according to their size as i) macro, ii) micro or iii) nano encapsulation.

Macroencapsulation Means filling a macroscopic container that allows considerable amounts of volume of PCM, from several millilitres up to several litres. These containers are often made of metal or plastic, which makes them very popular due to such containers being available in a large variety. In Figure 2.4 there's an example of two macroencapsulated PCM with a plastic foils package covered with a metallic layer to increse the package conductivity [4].

Figure 2.4: Examples of macroencapsulation; left produced by Climator, right produced by Dörken [4]

Microencapsulation The encapsulation of particles of 1 µm to 1000 µm diameter solid shell enclosing material in a solid or liquid state. Having a bigger surface area to volume ratio, increases the heat transfer and allows for easier charges and discharges of energy. This encapsulation type results mainly from physical processes like spray drying, centrifugal and fluidized bed processes, or coating processes. Microencapsulated PCM are available for example as fluid dispersion or dried powder that is incorporated directly into the feature's material [8].

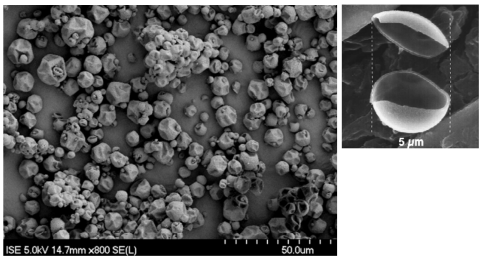

Figure 2.5: Electron microscope image examples of microcapsules filled with PCM [4]

Nanoencapsulation This is one of the most recently developed techniques to encapsulate the PCM into construction materials. The PCM included in this category convey dimensions under 1 µm. Their unusually high surface area to volume ratio, facilitates their thermal exchanges with its outer environment. However, since the shell of a NanoPCM is obviously much thinner than any of the other types of PCM, its compactness and toughness is considerably harder to achieve. Also, it is usual to find supercooling phenomenon in NanoPCM. The extent of this behavior relates to the contact between the core's and the shell's materials [9].

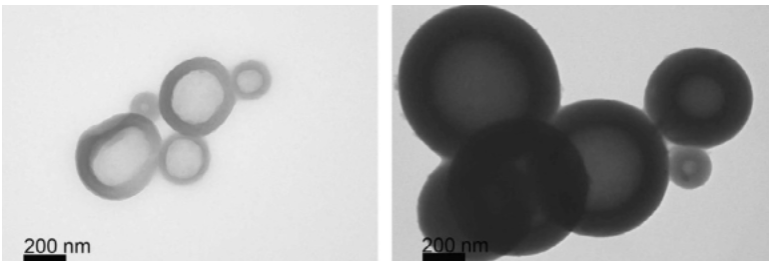

Figure 2.6: Transmission Electron Microscopic image examples of nanocapsules filled with PCM [9]

Shape-Stabilized Another way to integrate PCM is by mixing it with two supporting materials. This composite is called a Shape Stabilized Composite PCM (ss-CPCM) or shape stabilized PCM.

One of the supporting materials is a porous material used to prevent leakage and the other is a nano-material that improves the thermal characteristics of the mixture.

The setback of adding materials to PCM is their non-participation as energy storaging volume. That decreases the energy storage capacity of the composite in comparison to the original PCM sample [10].

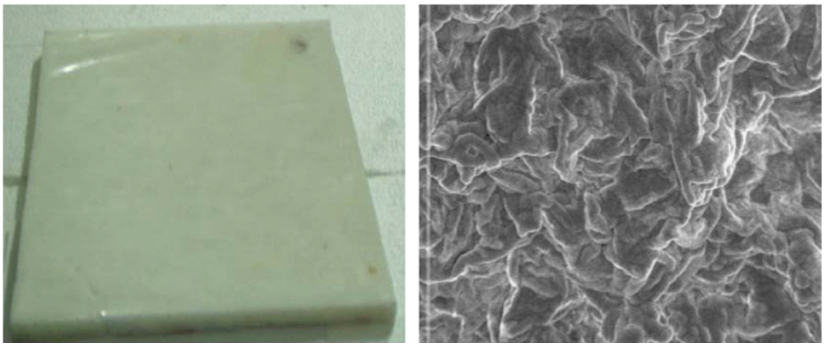

Figure 2.7: left: Shape-Stabilized PCM plate; right: Scanning Electric Microscope image example of Shape-Stabilized PCM [10]

Chapter 3

Literature Review

Presently a large number of articles are available containing research and developments related to Phase Change Materials, as well as their storage properties and incorporation techniques. It was in 1983 that the concept of using materials with high latent heat as energy storage systems was considered by Abhat [11], turning what was then only an interesting concept, to the foundation of a journey that promised to lead to a new reality.

Notwithstanding of his achievements, the pioneers of its employment in building applications went on to be Hariri and Ward [12], a few years later. They presented the first review of thermal storage systems specifically with the intent to optimize housing efficiency.

3.1 Building Applications Incorporating PCM

Throughout the years, many different solutions have been designed and refined around housing features that can incorporate this methodology for free cooling, heating or energy peak load shifting.

A brief introduction across the range of those applications will be made, and a more detailed state-of-the-art will then be presented relating to pavement applications only.

3.1.1 Walls

One of the most important heat gain sources of a building is its envelope due to its solar exposure throughout the day. This fact turns this constructive solution into one of the most desirable to incorporate PCM.

By incorporating these materials in the concrete of a building, an increase of its thermal inertia is verified. So, a reduction of the building's thermal conductivity allows for a considerable upgrade of its thermal performance, delaying and expanding the rhythm and interval of discharge.

However this method affects negatively the charge/discharge cycles of the storage system because of the low conductivity of the surrounding materials. As well as the integrity of the structure, and as a result there is a limited amount of PCM that can be added with this methodology [8].

In Figure 3.1 an example of a wall with integrated macroPCM filled pipes associated with an active system of water cooling can be observed.

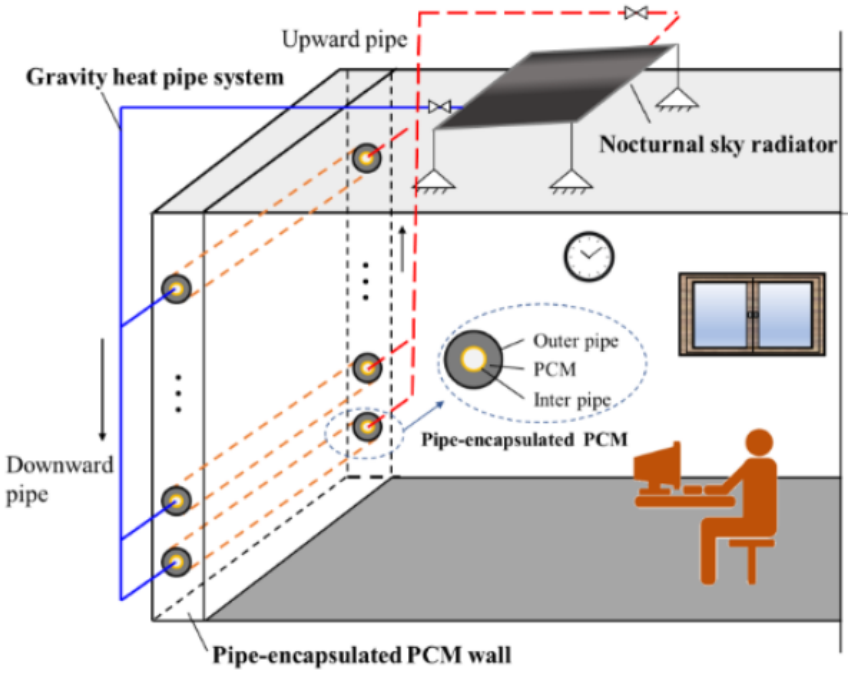

Figure 3.1: Example of Structural Walls PCM applications [13]

3.1.2 Wallboards

As the number of lightweight buildings rises in most countries around the world, the increase of energy consumption grows along with it, due to its particular characteristic of not providing as much natural thermal comfort to the user as a regular concrete construction.

The implementation of PCM based TES on their envelope, through wall covering boards of micro and nanoencapsulated PCM is one of the most investigated solutions to enhance the energy efficiency of this type of buildings. Also, unlike the previous case of structural walls, wallboards do not change the existing construction materials, instead, a component considered to be an economic substitute to standard thermal mass, is added to the existing installation [14].

Even though this application is mostly used in lightweight buildings, it can also be added to conventional construction. The example of Figure 3.2 is an application for cooling purposes. It increases the thermal inertia of the building, not allowing its interior to heat as much, but in which the energy absorbed is released back into the external environment, without the need to reuse the absored energy to heat its inside.

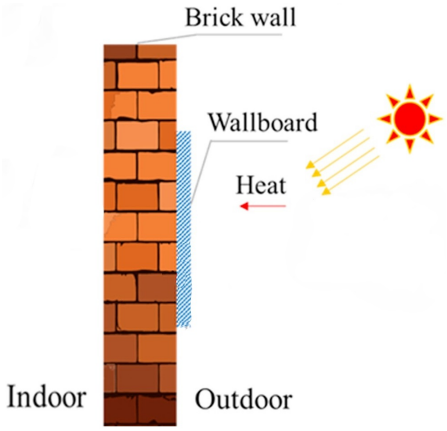

Figure 3.2: Example of PCM wallboards application on conventional construction [15]

3.1.3 Trombe Walls

A trombe wall is a sustainable architectural technology system that absorbs solar energy during solar hours, but it relies on sensible heat storage. Consisting of a high absorptivity wall placed behind a glass, at a distance that allows for air entrapment between the two. Thus retaining the heat income, possibly to take advantage of, or to release, according to heating or cooling needs, respectively.

Complemeting this construction feature with the incorporation of PCM is highly attractive due to the high potential of thermal energy storage. In Figure 3.3 the previous presented solution, PCM wallboards, was applied on the wall component of this system [14].

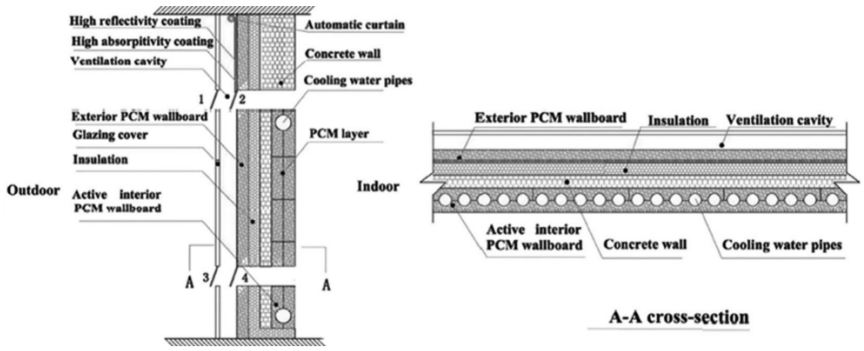

Figure 3.3: Example of a PCM ventilated trombe wall application [14]

3.1.4 Glazed Windows

Analysing building features with a great impact in the thermal comfort of a building, glazed windows play a big part of heat gains and losses, in summer and winter seasons, respectively. Moreover, their incorporation has been increasing in number and size when considering contemporaneous design and architecture.

However, employing PCM in this particular envelope is also one of the hardest techniques. In the application of PCM of Figure 3.4 some obstacles were faced. Given that PCM reflect, absorb and conduct light differently at different energetic states and wavelengths. That introduces a special requirement to not only, not harm the sensitivity of the human eye but also to not obliterate the goal of glazed facades in the first place, an unobstructed view and an allowance of brightness [16] [8].

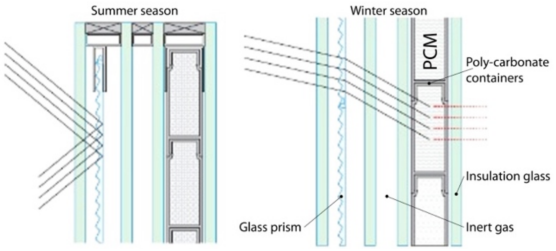

Figure 3.4: Example of a PCM glazed window PCM application [17]

3.1.5 Shading Devices

One of the oldest and most simple solutions available to minimize the impact of glazed windows in a building's indoor thermal temperature is to add an external or internal shading element. However, the amount of heat that shading prevents the building from gaining, was not being stored to take advantage of, when needed.

Inspired in that, another PCM feature was developed, by incorporating the PCM into the shading devices instead of the glazed windows. This solution avoids the physical requirements addressed previously, and increases the resistance between the energy storage system and the outside environment, allowing slower discharges into the desired heating space [16] [8].

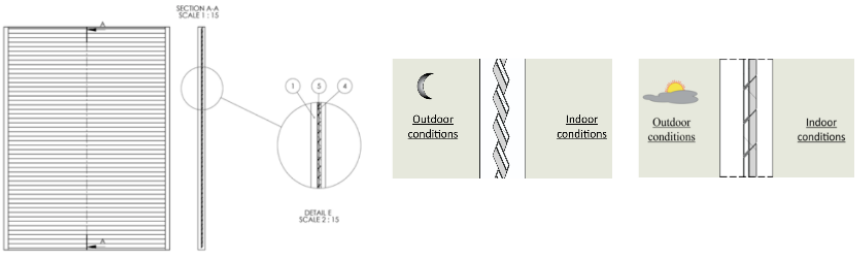

Figure 3.5: Example of a PCM Window Shutter PCM application a) Overall scheme; b) position of discharging; c) position of charging [16]

3.1.6 Solar Wall Collector

Solar collectors are already a widely used environmentally friendly method to water heating. However, since solar exposure does not usually overlap with the peak of need for heated water in typical family households, incorporating PCM into this kind of systems allows not only to store more energy, but also to store it until the consumption peak period, enhancing it's overall efficiency.

Nevertheless, because this active approach still depends on the intensity of solar radiation they are only valid as a support to conventional gas or electric water heating systems and not a sustainable solution on its own [5].

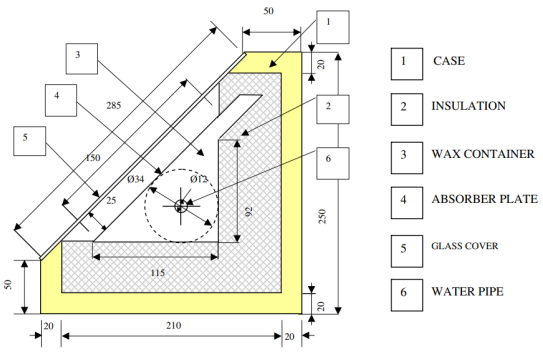

Figure 3.6: Schematics of an cross section of an experimental apparatus of a PCM Solar Wall Collector application for water heating [18]

3.1.7 Floors and Ceilings

Other building features that can take advantage of PCM are the floors and the ceilings. Even though the solar coverage may not be as intense and long-lasting or even exist at all, as in some of the previous solutions presented, these locations are privileged when talking about both surface area and the possibility of associating them with other heating or cooling active systems. It's even possible to combine the two features and enhance the overall efficiency like the example of Figure 3.7.

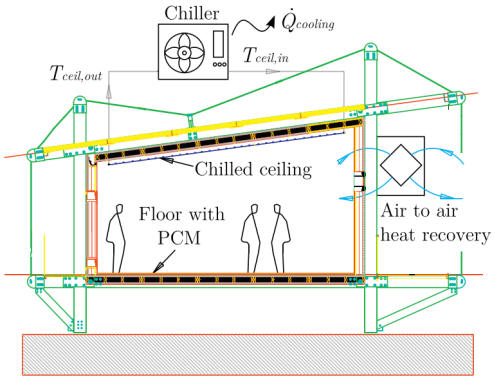

Figure 3.7: Example of PCM Floor and Ceilings application [19]

3.2 State of the Art on PCM Floor Applications

The biggest considerations to be made when discussing an application like PCM floors, lie with 1) selecting the most suitable parameters of a PCM, 2) its incorporation method, 3) the floor's configuration and 4) the operation of the system itself and eventual associated systems [20]. To understand the progress that has been made to refine this application method, the main stages of its R&D will be presented next.

1999 In 1999, with the increase of underfloor heating technologies, Farid *et al.* [21] investigated, resorting to a computer simulation, the potential of a 30 mm PCM layer applied in between an electric heating layer and the floor tiles like illustrated in Figure 3.8. That way increasing the thermal mass of the floor and hoping to shift the energy consumption to an off-peak period.

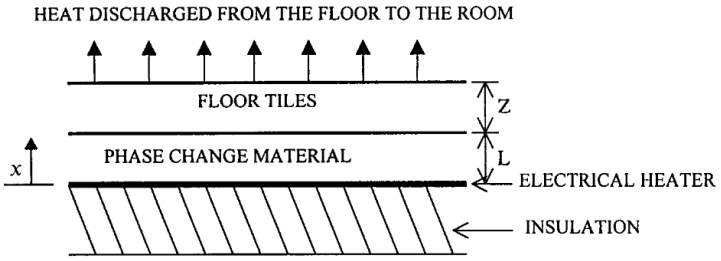

Figure 3.8: Sketch of the underfloor heating system with PCM layer and electric heating, 1999 Farid *et al.* [21]

It was determined by solving the un-steady state heat conduction equation with the explicit finite differences method, that it was viable to use this solution to provide uniform heating throughout the day, while only providing thermal energy during 8 hours in the previous night. However the floor surface temperature resultant of this approach was found unfit for human comfort during part of the discharge time.

2001 Just a couple of years later, Farid *et al.* [22], tried to improve the previously obtained results and mitigate the human discomfort associated with it. By assembling an experimental set up like the one in Figure 3.9, changing both the integration method of the PCM, incorporating them microencapsulated into the concrete underfloor during its construction, and the thermal energy provider method, that became water based instead of electric.

While storing energy during the off-peak electricity period for the same 8 hours and still being able to discharge throughout the majority of the next day. The changes that were made from the previous article to this one, allowed for thermal comfort, given that they lowered the temperature fluctuation and maintained a surface temperature close to 24°C.

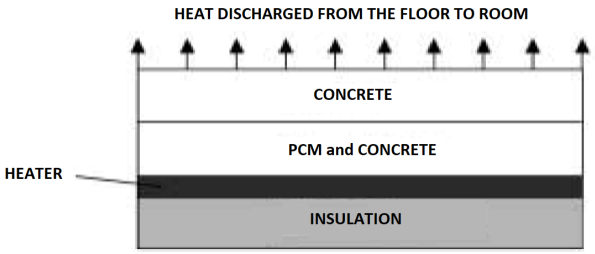

Figure 3.9: Sketch of the concrete underfloor system with microencapsulated PCM, 2001 Farid *et al.* [22]

2004 Two of the biggest problems associated with applying this type of TES systems in encapsulated form, is the leakage that occurs frequently, consequence of long term use and the added resistance of the encapsulating material. In an attempt to overcome that, Lin *et al.* [23] experimented with a different form of incorporation as observable in Figure 3.10, by using a compound material underfloor plate, associated with an electric heating system. These SS-PCM plates' experiments revealed to be valid and the obstacles that were inherent to the use of encapsulation were this way, extinguished.

Figure 3.10: Pictures of an experimental underfloor heating system with macroencapsulated PCM, 2004 Lin *et al.* [23] ; left: electric layer; centre: SS-PCM layer; right: wood layer.

2005 Following those positive results, Lin *et al.* [24] complemented his research on shape-stabilised PCM plates, resorting to numerical simulations, with an underfloor system like Figure 3.12, to broaden the number of variables under analysis, that will influence the general system and it's consequent results.

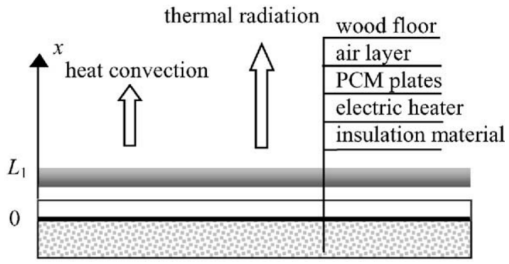

Figure 3.11: Sketch of the underfloor layers used for numerical simulation, 2005 Lin *et al.* [24]

2007 Lin *et al.* [25] , who had previously delivered other studies [23] [24], presented a new research with experimental results and numerical simulation. A new electrical floor heating system with ductless air supply and SS-PCM plates, such as in Figure 2.7.

What motivated this research was the fact that previous solutions were not optimized to buildings where no space heating is required during the night period, for example office buildings. Due to the reduced service hours when comparing to households, the PCM remained at the phase change temperature throughout the whole utilization period. As a result, the indoor temperature was found to increase efficiently assisted by the air chambers.

Figure 3.12: Electrical heating system with ductless air supply and SS-PCM; Left: Sketch of the underfloor layers; Right: Picture the experimental setup of the underfloor system, 2007 Lin *et al.* [25]

2011 However, after three decades of developments, Cerón *et al.* [26] argued that no economically valid and easily installable solution existed yet, and so a prototype of a block tile incorporating macropackaged PCM, as in Figure 3.13, was designed to cover the floor of a workspace without the need of major construction intervention or active heating or cooling systems.

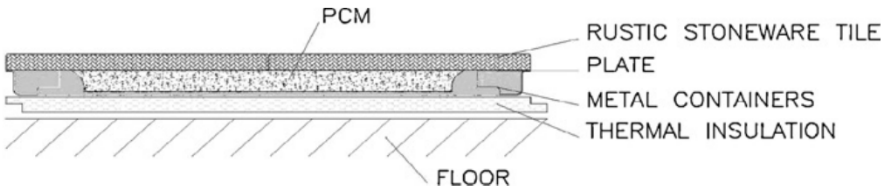

Figure 3.13: Sketch of the underfloor heating system with macropackaged PCM , used for experimental tests, 2011 Cerón *et al.* [26]

As expected, comparisons on the superficial temperatures of the tiles were made with similar ones that did not contain thermal energy storage systems. In this specific experimental article, also the existence, or not, of blinds and the distance of the tiles to the glazed windows, was evaluated due to its variable solar radiation exposure.

Results on the PCM tiles closer to the windows, showed an ability to maintain a higher superficial temperature than the regular tiles during the whole night period if the previous day was sufficiently sunny, as well as the capacity to maintain a much lower temperature at the peak of sun exposure. However, because no other source of thermal energy was considered other than the solar exposure itself, the tiles that were not under direct radiation were not found to have a good enough performance to justify its employment for heating purposes.

2011 In the same year that the previous experimental article was published, another numerical one, by Jin *et al.* [27], was too. Considering a different methodology, incorporating not only two phase change material layers, instead of one, but also the usage of hot water as a thermal energy provider.

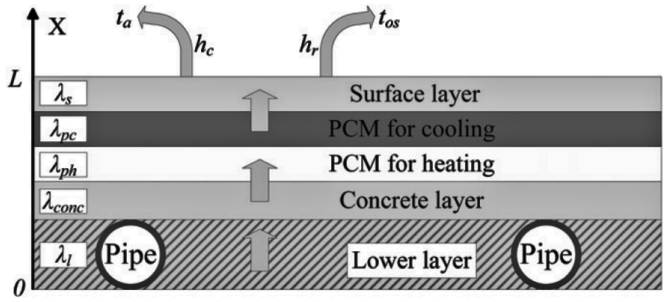

Figure 3.14: Sketch of the underfloor heating system with a double PCM layer used for numerical tests, 2011 Jin *et al.* [27]

In this case both PCM layers have different melting temperatures, one that is more suitable for heating and another for cooling. As to the water heating process, a heat pump or a chiller, is considered to work in the off-peak hours servicing a water pipe, placed in the concrete under the thermal storage layers, that extends across the length of the floor. Due to the addition of a PCM layer dedicated exclusively for each process, the efficiency of the heating procedure which so far had not been as satisfactory in most studies as cooling, increased by 40%.

2014 Few years later, Huang *et al.* [20] combined both numerical and experimental procedures in the designing and development of a new underfloor configuration. Employing a capillary water system, that supplies the thermal energy to the macropackaged PCM layer in a more homogeneous and efficient way, as Figure 3.15 suggests. Also, instead of an electrical process for water heating, this system was coupled with a solar water heating structure that would charge the PCM during the day, so that the stored energy could be released in the night time.

However, depending on this solar system alone was doomed unrealistic, given the outside weather may not be always favourable to solar heating, and so it was advised that in further studies the addition of other hot water control strategies should be considered.

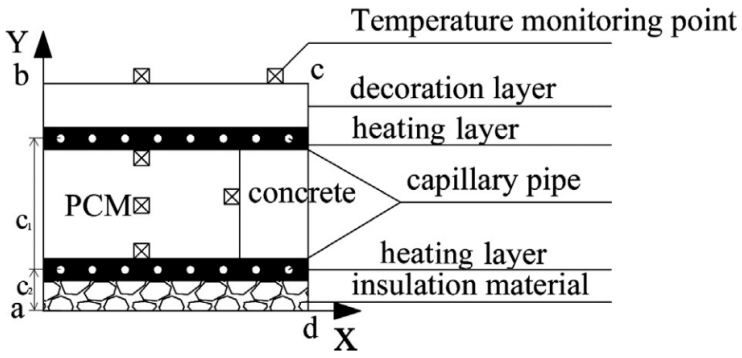

Figure 3.15: Sketch of the underfloor capillary heating system used for both numerical simulations and experimental tests, 2014 Huang *et al.* [20]

2016 Based on the double layer concept [27], Xia *et al.* [28] developed a model with the aim of improving the heat transfer performance between the thermal storage system and the water, by changing the location of the pipes that were initially considered to be inside the concrete foundation of the system, to be considered now as a capillary system that passes through the PCM layers.

This way, the water pipes are surrounded by the material that is intended to charge in the first place, avoiding energy losses in between the energy source and desired storage receiver, as Figure 3.16 demonstrates.

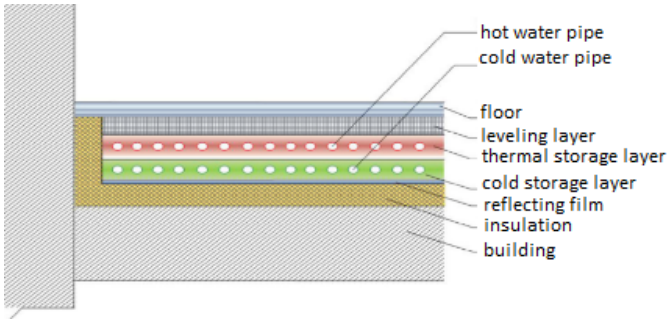

Figure 3.16: Sketch of the double layer PCM underfloor with cappilary water system, 2016 Xia *et al.* [28]

It was also considered that the pipes that cross the highest melting temperature PCM layer were exclusively for hot water passage and the ones in the lower melting temperature layer to cold water, as well as evaluated the impact and general efficiency of switching those layers' order.

By allowing the presence of both hot and cold water in the system, the system becomes more suitable for both summer and winter usage, since it's possible to control both the absorbtion and releasing of energy, from and to the enviroment, respectively.

2017 When Zheng *et al.* [29] studied the design and optimization of a Zero Energy Consumption Residential Building, also known as ZERB, a PCM floor was implemented along with other passive systems as Figure 3.17 shows.

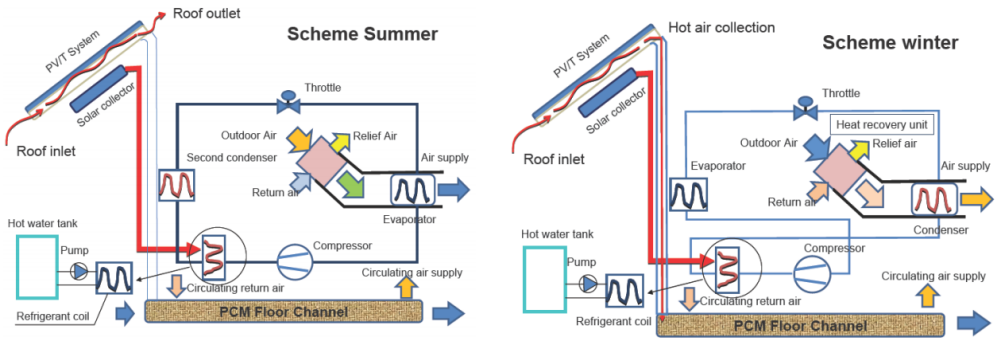

Figure 3.17: Schematics of the ZERB's components and opearation during heating and cooling seasons, 2017 Zheng *et al.* [29]

In this article, an energetically independent and self-regulating construction was modelled and optimized. Unlike the previous examples where the application of PCM, with or without the association of other active or passive systems, was designed to lower the total amount of energy required of the external power grid.

In this case, this energy storage system was deemed viable to contribute to a self-governing standalone structure. However, because multiple systems were analysed functioning simultaneously, results cannot be attributed to the PCM alone.

Chapter 4

Modelling and Numerical Simulation of the Phase Change Material's Application

To model the behaviour of the PCM when subjected to energy transfers, an article by M. Mahdi, H. Mahood *et al.* from 2021 was used to calibrate and validate the CFD numerical model [30]. The article studies different scenarios of PCM integrated systems and evaluates the influence of induced convection flows in the melting rate of its volume. The article also displays all the information to model the geometry, set material parameters and simulation setup definitions that are needed, as well as graphics and illustrations of the results that will be used for comparison with the obtained data, as this chapter will demonstrate.

4.1 System Description

The system used in the article can be described as a Shell and Tube Heat Exchanger (STHE), which means the cross section of the pipe enclosing the volume of PCM is crossed by three pipes containing running water, serving as Heat Transfer Fluid (HTF). The article presents four different cases, in each of them the location and configuration of the pipes changes, as visible in Figure 4.1. To validate the obtained results, case B was selected.

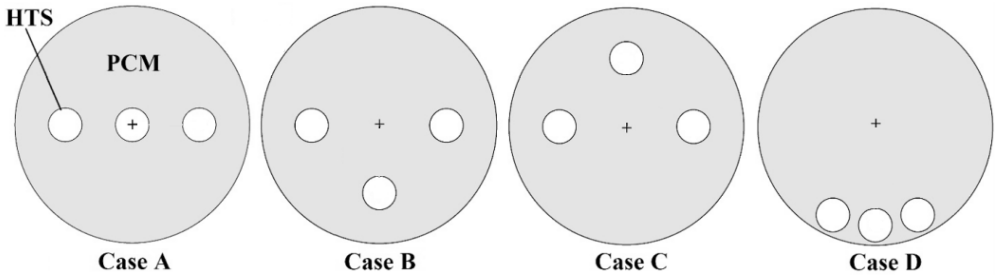

Figure 4.1: Schematic view of the four different cases used for comparisson in the original article [30]

Even though case D was the one who developed the shortest total melting time, case B revealed the quickest melting rate for the majority of the simulation time, as well as presented the geometry that is the most consistent with both the STHE principle and the study of the influence of convection flows effect, by having the pipes more spaced and distributed on the geometry in an upside down triangular shape.

4.2 Numerical Definitions

To set up the model with the correct settings and to input all the required information, Ansys® user guide was heavily used [31], with an emphasis on its section regarding the setup for solidification and melting analysis procedure [32].

4.2.1 Geometry

Its geometries' measurements are, 1) the outside diameter of the PCM shell which is $70mm$, and 2) the three Heat Transfer Surface (HTS) with $10mm$ of diameter each. The 2D geometry was modeled resorting to the planar surfaces feature of a Computer-Aided Design (CAD) Software, SolidWorks2020® and can be visualized in Figure 4.2.

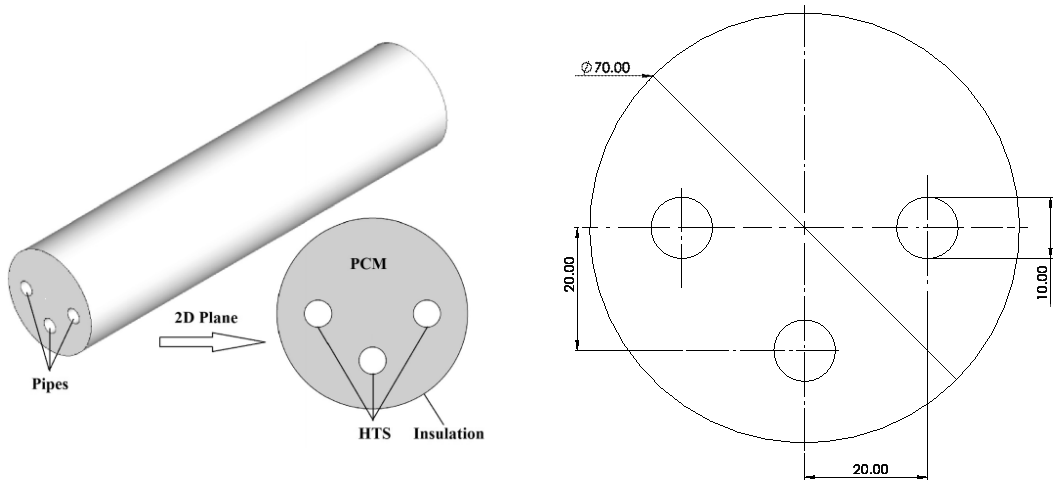

Figure 4.2: Left: Article's 3D geometry depiction [30]; Right: SolidWorks® sketch of the geometry model used for numerical validation of the PCM behaviour

4.2.2 Mesh

The geometry was imported in .IGS format from SolidWorks® Student Version 2020 and the mesh developed for the simulation, Figure 4.6, was performed in the meshing component of the Fluent analysis system of Ansys® software.

To ensure the right level of detail of the simulation, the maximum size of the mesh's elements was evaluated with the intention that the size of the elements was as little as possible, in order to obtain the most detail, without the total number of elements in the mesh becoming too high, increasing computational time unnecessarily and possibily overflowing the simulations. After analysing Figure 4.3 which relates the size with the number of elements the software generates, the mesh element size was set to $0.5mm$.

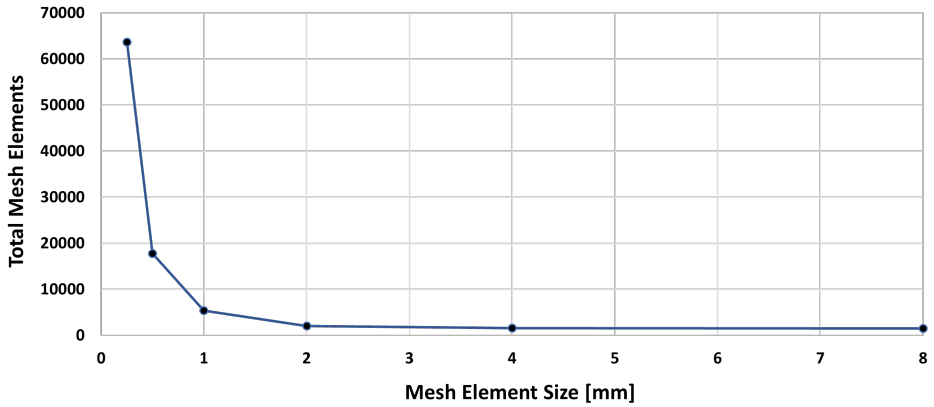

Figure 4.3: Graph that relates elements' size and total number generated by the software

There were also inflation layers applied around the HTS edges. This feature creates thin elements to better analyse the interaction and energy transfer between the HTF and the PCM. The impact of the number of layers, as well as their respective growth rate, in the overall mesh quality was studied and is presented in Figure 4.4. Because the thin elements created by the inflation feature do not present an element quality similar to the rest of the elements in the mesh due to their elongation, it's predictable that the higher the number of layers or their growth rate, the lower the orthogonal quality of the overall mesh, as supported by the obtained results.

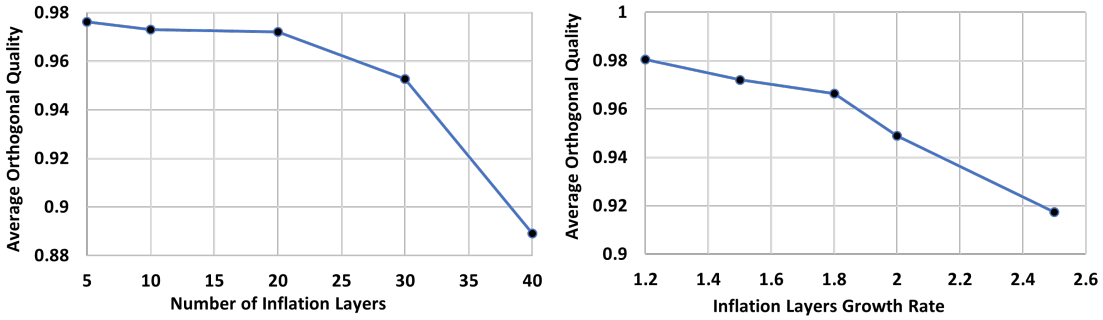

Figure 4.4: Inflation Parameters Evaluation, Left: Number of layers; Right: Growth rate

Even though increasing the size and number of elements resultant of the inflation application, lowers the quality of the mesh, it is beneficial to observe the energy transfer that occurs in them with more detail. When considering the maximum number of layers that can be applied in the mesh without compromising its quality, we can conclude that the orthogonal quality does not present a significant variation until the 20 layers. The same does not apply for the second inflation parameter, in which quality decreases significantly with every growth rate increase considered.

In order to study the equilibrium, a graph of the mesh quality when relating the two parameters, as Figure 4.5, was required. For each growth rate value considered, a respective 10 and 20 number of layers was evaluated.

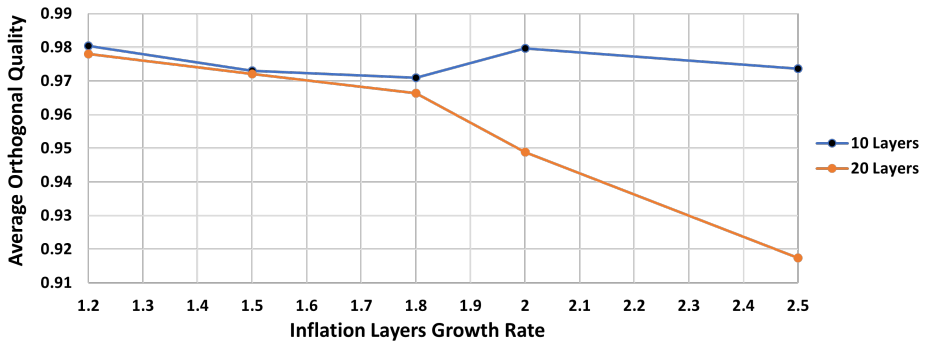

Figure 4.5: Orthogonal quality relative to combined parameters

The chosen combination of the parameters above was a number of layers of 20 and a growth rate of 1.5, and so the final mesh adds up to a total of 17777, very close to the 16000 that the original article classified as the optimal elements number. Both the inflation layers and the general mesh results are illustrated in 4.6.

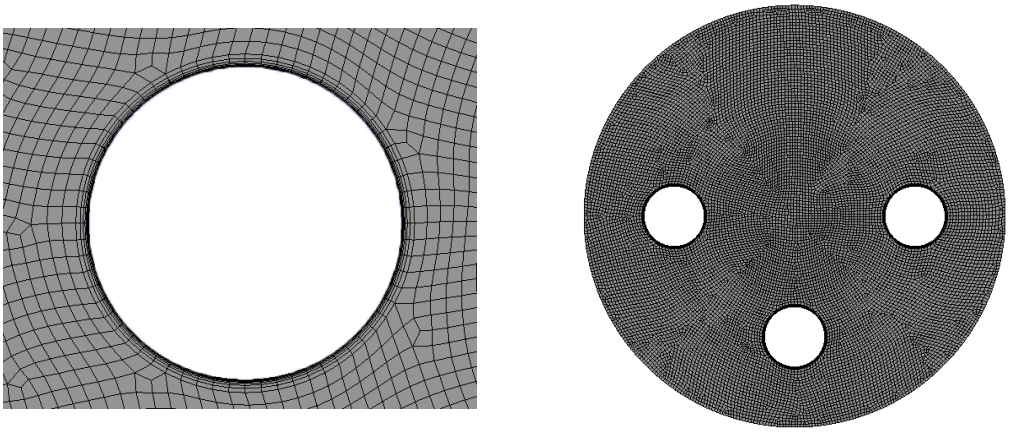

Figure 4.6: Left: Zoom in of the inflation layers; Right: Final mesh of the geometry's surface

Once the meshing process was complete, quality control parameters like orthogonal quality, element quality and skewness were verified, to guarantee the mesh would ensure a high quality level simulation.

Orthogonal Quality The average orthogonal quality of the mesh is computed between each element in relation to their neighbours, with resource to vector mechanics. Calculations are made to determine the highest angular deviation of the vector connecting two adjacent cell centres and the surfaces normal to the vector of their common face. Values range between 0, where the elements appear squished on top of each other, and 1 where they seem to fit in, maintaining their perfectly square form [33].

In Figure 4.7, we can observe a histogram of the orthogonal quality of the elements of the mesh. The average value of this parameter is 0.972 and 95% of the elements have a value over 0.9.

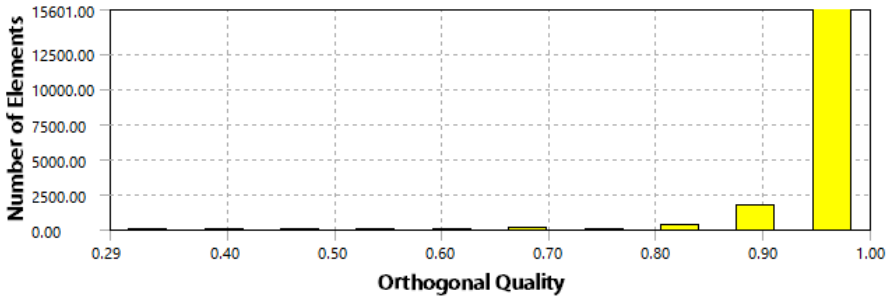

Figure 4.7: Orthogonal quality graph of mesh elements

Element Quality This type of mesh metric relates to each element at a time and it ranges between 0 and 1. The closer the values are to 1, the closer the shape of the element is to a perfect square. The calculation formula for this parameter is described in equation 4.1, where, for the type of elements used, the constant C equals 4.

As expected and verified, the elements highligthed in pink on the histogram of Figure 4.8 result from the inflation feature. These elements have lower element quality because inflation changes their shape, stretching them along the curvature of the edge, and consequentially the element quality of those elements decreases significantly. On the bottom of the same Figure we can observe a detailed view of the elements that corresponde to these lower values [34].

$$Quality = C\frac{Area}{\Sigma(EdgeLength)^2} \tag{4.1}$$

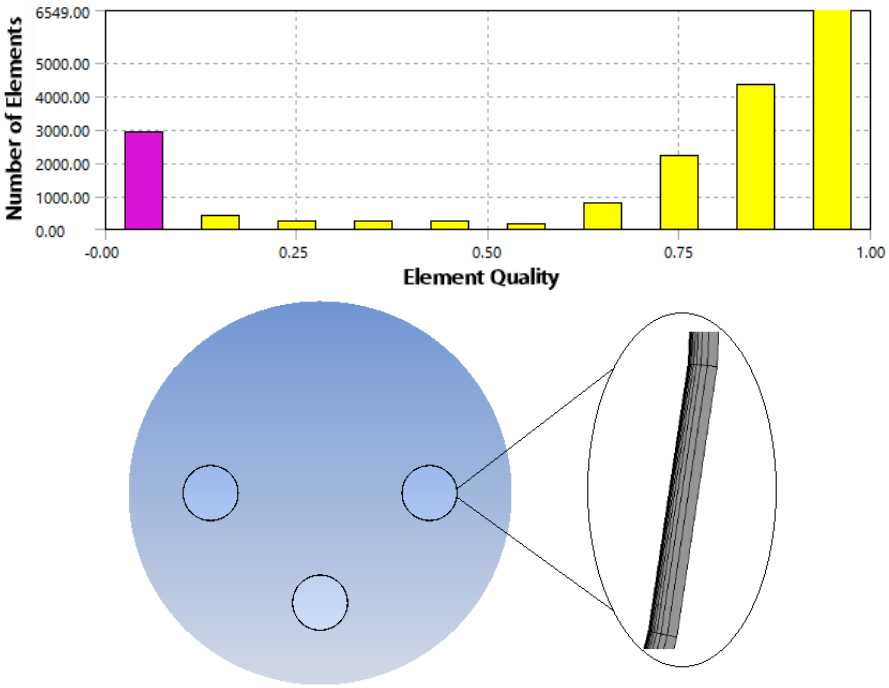

Figure 4.8: Element quality graph of mesh elements

Skewness This parameter also determines how close to an ideal cell or element, the analysed element actualy is, in an equilateral and equiangular point of view. However, unlike the previous mesh metrics analysed, in this case a value near 0 is preferable, given that it indicates an equi-cell, and a value of 1 indicates a completely degenerate one [35].

There are two methods for measuring skewness. Based on the equilateral volume, that is not applicable in 2D mesh, and based on the deviation from a normalized equilateral angle.

$$max\left[\frac{\theta max - \theta e}{180 - \theta e}, \frac{\theta e - \theta min}{\theta e}\right] \quad (4.2)$$

Variables:

- θmax = largest angle in the cell
- θmin = smallest angle in the cell
- θe = angle for an equiangular cell (Square mesh = 90^{o})

The results for the case-study displayed in Figure 4.9 show that over 92% of the elements of the mesh have a skewness within the very good interval value (<0.25) and 99.9% in the good interval (<0.5), defined by Fatchurrohman et al in [36].

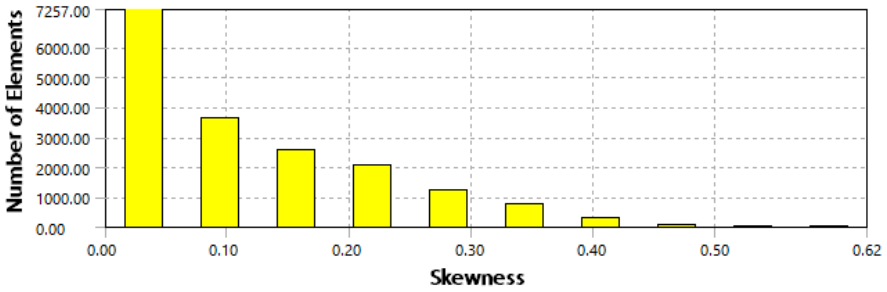

Figure 4.9: Skewness graph of mesh elements

4.2.3 Solver and Models

The settings for the type of solver used were pressure-based, more relevant for incompressible and low-speed flows, which unlocks the Navier-Stokes solution algorithm. Also, the simulation is time-dependent which means the option transient is required. Both of these parameters implementation can be observed on the left of Figure 4.10.

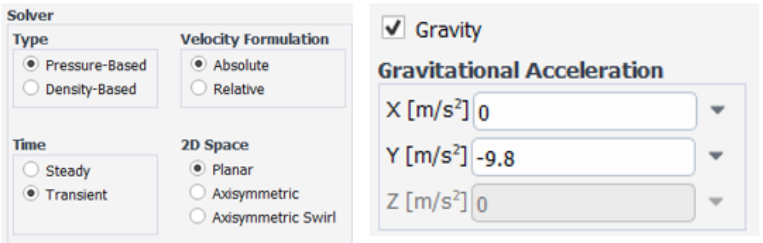

Figure 4.10: General solver definitions

The temperature variation within the geometry influences the density value of the material, which in turn requires the gravity feature to calculate natural convection and buoyancy phenomenon that influences the melting process, applied as on the right of Figure 4.10.

Mass conservation equation for incompressible flows:

$$\nabla . v = 0 \tag{4.3}$$

Variables:

- v = Fluid velocity

Momentum conservation equation:

$$\frac{\delta v}{\delta t} = -(v.\nabla)v + \nabla.(\rho_v \nabla v) - \frac{1}{\rho}\nabla p + g\beta(T - T_0(j)) + S \tag{4.4}$$

Variables:

- ρ = Density
- p = Pressure
- g = Gravity
- ρ_v = Dinamic viscosity
- S = Mushy zone parameter

Energy conservation equation:

$$\frac{\delta}{\delta t}(\rho H) + \nabla.(\rho v H) = \nabla.(k \nabla T) \tag{4.5}$$

$$H = h + \nabla H \tag{4.6}$$

$$h = \int_{T_0}^{T} C_p dT \tag{4.7}$$

$$\nabla H = \lambda L \tag{4.8}$$

Variables:

- H = Enthalpy
- h = Specific enthalpy
- k = Thermal conductivity
- c_p = Specific heat capacity
- L = Latent Heat
- λ = liquid fraction

Viscous Model: Laminar No value for the HTF flow rate or velocity is involved in the reference case simulation, making it impossible to calculate a Reynolds number. However, since the simulation is two dimensional and the interface between the HTF and the PCM is an edge, the influence of the flow's turbulence condition is irrelevant, only its temperature, which is constant, will influence the results. This way, the simulation was set to follow a laminar flow of water inside the pipes.

Energy Model This model enables the ability of the software to perform calculations with energy data during simulation. It is required to perform heat transfer calculations.

Solidification and Melting Model In order to simulate the phase change process that will occur during computation, and to unblock material properties such as the latent heat storage capacity and the solidus and liquid temperature, this model is required.

This model unlocks an enthalphy-porosity technique, which means a variable called liquid fraction , λ , represents the percentage of elements in the mesh that have reached melting temperature.

The liquid fraction is computed at each iteration, based on an enthalpy balance. This method also introduces the mushy zone parameter, S, which measures the amplitude of the damping and was set at $10^5 kg/m^3 s$. Mushy zone is a semi-solid region existing as an interface between the melted and the un-melted region of PCM [37]. The higher the mushy parameter is, the quicker the transition of the material to solid state.[38]

When a fluid changes temperature, a flow created by the variation in it's density can be induced due to gravity. In this case the density of the PCM is defined according to Boussinesq model which sets the density (ρ) as a function of temperature. This method is faster to converge and treats density as a constant value in all solved equations, except for the buoyancy term in the momentum equation [39].

$$(\rho - \rho_0)g \approx -\rho_0 \beta (T - T_0)g \qquad (4.9)$$

$$\rho = \rho_0 (1 - \beta \nabla T) \qquad (4.10)$$

Variables:

- ρ_0 = Constant Density
- T_0 = Operating Temperature
- β = Thermal Expansion Coefficient

4.2.4 Material Definitions

The only material required to simulate this working system is the PCM, which in this case is a fatty acid. Its properties' values, present in the original article, were manually inserted in their respective fields, as shows Figure 4.11.

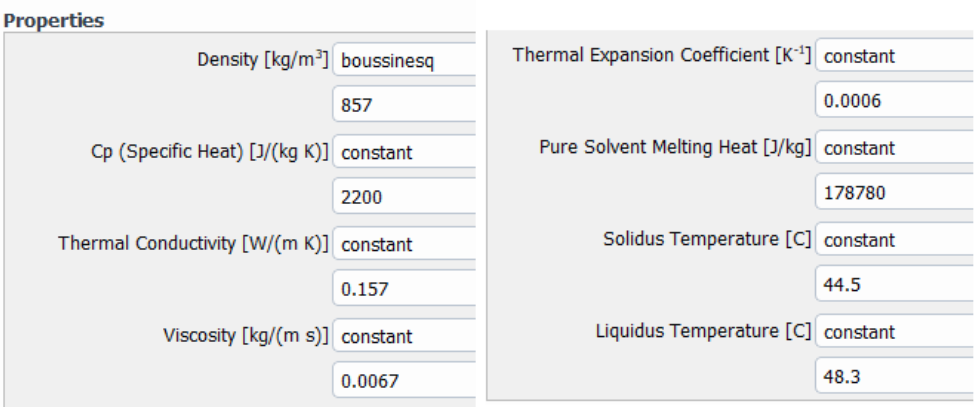

Figure 4.11: PCM properties

4.2.5 Boundary Conditions

The initial temperature is set to 25°C for the entire domain. To simulate the water flow in the three pipes, a constant temperature of 70°C was set in the HTS that encloses the flow. The outer edge of the geometry is adiabatic, and for that the heat flux was set to 0 W/m^2. Both boundaries can be seen highlighted in yellow in Figure 4.12.

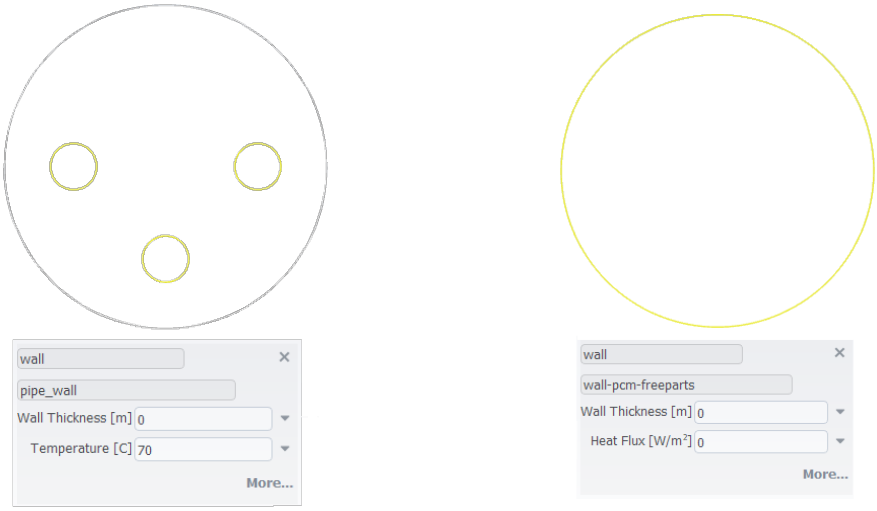

Figure 4.12: Outer edge boundary condition

4.2.6 Solution

Methods The original article specified the SIMPLE algorithm for pressure-velocity coupling, PRESTO algorithm for the pressure term and second-order up-wind option for both the energy and momentum conservation equations.

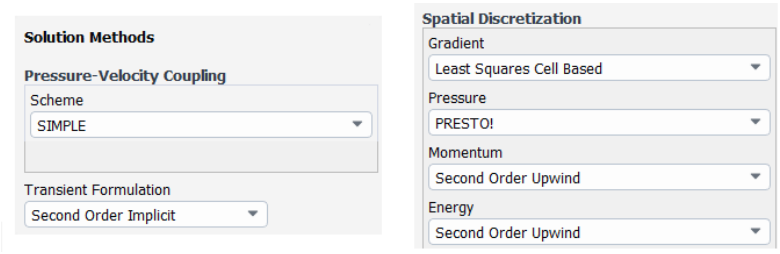

Figure 4.13: Solution Methods

Controls In order to turn the convergence of the simulation into a more stable process, the following under-relaxation factors were set.

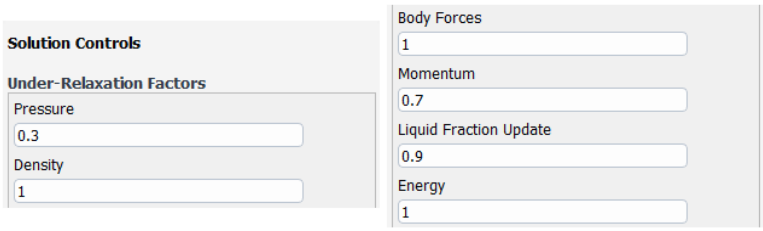

Figure 4.14: Solution Controls

Residual Monitors The convergence criteria was set to the values of 10^{-4} for continuity, 10^{-5} for the velocity components and 10^{-7} for the energy equation.

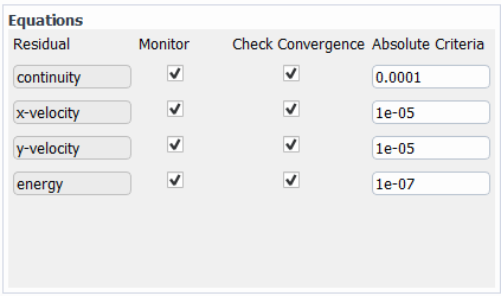

Figure 4.15: Solution Monitors

Calculation The time step size used to perform the calculations was 0.1 seconds for as long as the liquid fraction variable was different than 1, which in practical terms summed up to 54628 seconds of simulation and 546280 iterations.

4.3 Model Calibration and Validation

In order to confirm the definitions used to simulate the phase change of the material and the energy transfer between the water and the PCM were validated, the data obtained from Ansys® simulations has to be compared to the original article's results. Because the original article presents their findings in both graphic form and illustrations, both a visual and mathematical analysis were conducted to establish a parallel between them.

The article's original plot, Figure 4.16, relates how the liquid fraction of the entire simulation domain develops over time, however only the results relating to Case B are relevant for validation purposes. The total simulation time for this configuration set in the original article was 112 minutes.

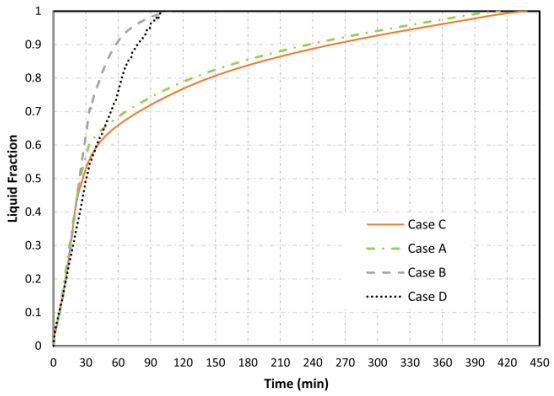

Figure 4.16: Plot of PCM liquid fraction on the 4 cases of study of the original article [30]

This graph was ran through an online software, *WebPointDigitizer* [40], so that the values of specific points could be extracted for comparisson with the obtained results, with the best possible accuracy. The overlapping red points on the left of Figure 4.17 were the selected time values to compare against the obtained results. On the right graph of the same Figure, the exact same procedure was performed for the obtained results. The total time for this simulation was 5462.8 seconds, which is equivalent to 91 min.

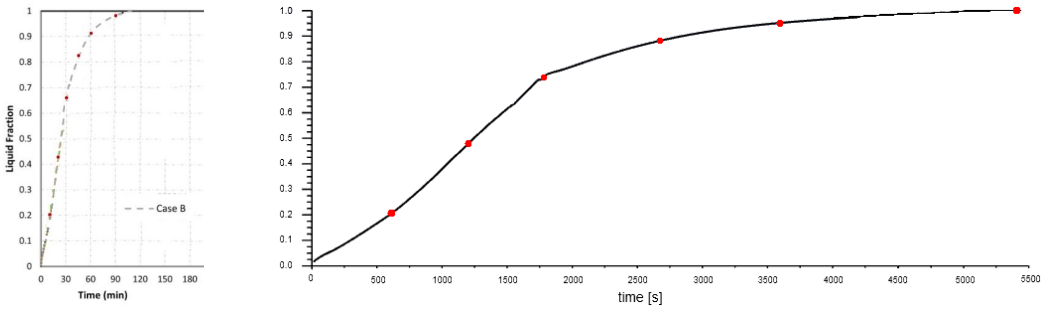

Figure 4.17: Reference points for comparisson

The 21 minute difference in the total simulation time, predicts that the phase-change process developed quicker in the attempt to replicate the original article than on the original results themselves. It is expected to find a steeper curve in the melting rate of the material, when superimposed on the original plot.

The following table (table 4.1), presents the results extracted from the data collected in the previous Figures and the relative error, at the respective instants, between those values and the reference ones. The overlap of the two graphics, Figure 4.18 provides a visual confirmation of the calculated error values and the expectation of a higher slope on the obtained values' curve. However, the curves describe a similar trajectory and both decrease their rates considerably around the 30 minutes mark.

Table 4.1: Liquid fraction values for reference times

Time [min]	**Reference Resutls**	**Obtained Results**	**% Error**
10	0.2034	0.2077	2.135
20	0.4283	0.4791	11.84
30	0.6605	0.7387	11.83
45	0.8256	0.8846	7.143
60	0.9127	0.9484	3.913
90	0.9816	0.9978	1.652

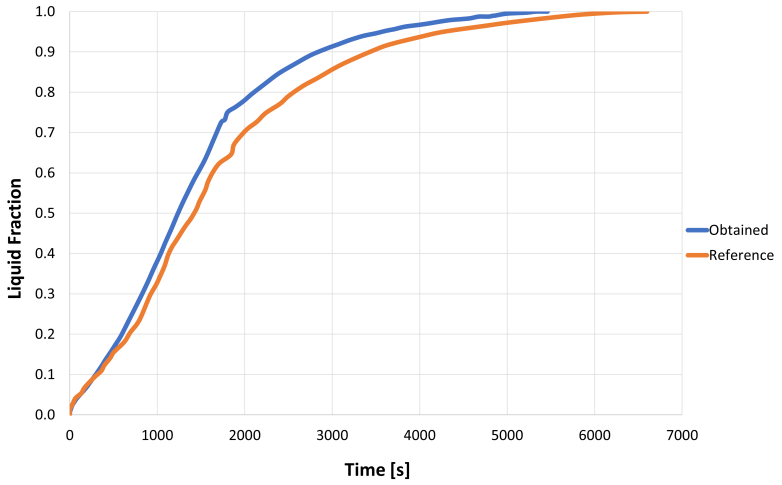

Figure 4.18: Reference vs obtained results

To further address and analyse the validity of the results, another error calculation formula is used to determine the proximity of the simulation's results as a whole and not at specific instants. For that, an article by Cipriano *et al.* [41] was considered, and the Goodness of Fit (GOF) criteria was calculated, equation 4.13. For that, both the Normalized Mean Bias Error (NMBE) and the Coefficient of Variation of the Root Mean Square Error (CVRMSE) were also determined, as shown in equations 4.11 and 4.12.

$$NMBE(\%) = \frac{\Sigma[y_r - y_o]}{n \times y_a} \times 100 \quad (4.11)$$

$$= 6.09\ \%$$

$$CVRMSE(\%) = \frac{\sqrt{\frac{\Sigma[y_r - y_o]^2}{n}}}{y_a} \times 100 \quad (4.12)$$

$$= 7.15\ \%$$

$$GOF(\%) = \frac{\sqrt{2}}{2} \times \sqrt{NMBE^2 + CVRMSE^2} \quad (4.13)$$

$$= 10.10\ \%$$

Variables:

- y_r = Reference Result
- y_o = Obtained Result
- n = Total Number of Terms
- y_a = Average Reference Result

The article recommends the GOF value to be under the limit of 11% to consider a simulation as calibrated. Since the assessed value respects the limit imposed, we can consider that this results are according to the criteria, and so the setup used for the model verification is considered valid.

Besides the liquid fraction graph used for validating the model, the original article provided the PCM temperature's and liquid fraction's contours, presented on the left of tables 4.2 and 4.3 respectively. Such data was also collected during the Ansys® simulation and is displayed on the right side, accordingly. The colormap options were also adjusted to the original article's properties, in the temperature contours colormap presents a minimum value of 25°C and a maximum of 70°C, with 10 equally intervaled colors.

The 10 minutes contours of obtained results for both liquid fraction and temperature are very similar to the original contours. The temperature of the induced convection flows are, however, a little higher in the obtained results which is consistent with the 2.135% error that was calculated in table 4.1.

For minute 30 we can clearly observe the difference in the rates of the progress of the two simulations. The obtained simulation is at a much more developed stage of the melting process, also consistent with the 11.83% from liquid fraction values table. On the temperature contours, the obtained results no longer presents any region at the initial temperature, unlike the original.

Also according to the error values, after 30 minutes the drastic difference between the two is mitigated throughout time, which is also visible on both temperature and liquid fraction contours.

Table 4.2: PCM temperature contours during different melting times for the reference (left) and obtained (right) study cases

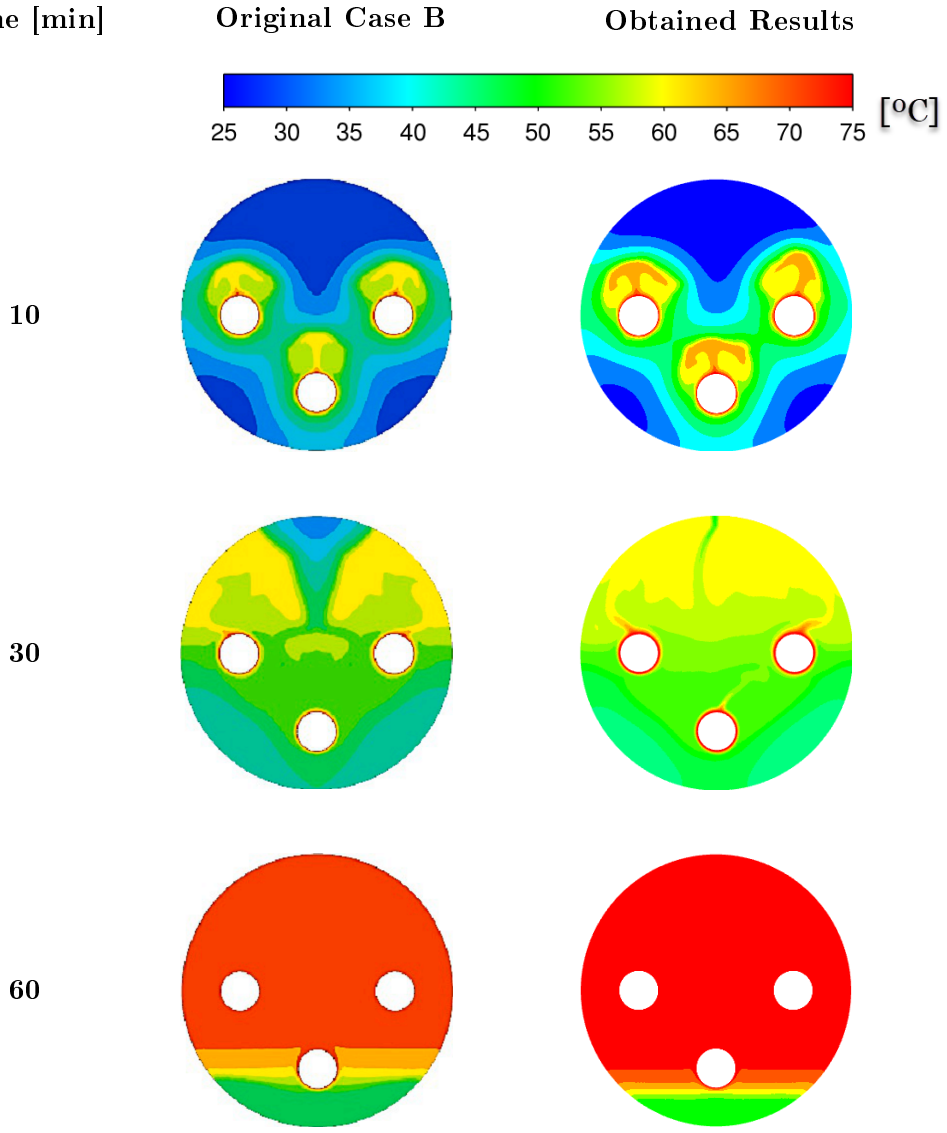

Table 4.3: PCM liquid fraction contour during different melting times for the reference (left) and obtained (right) study cases

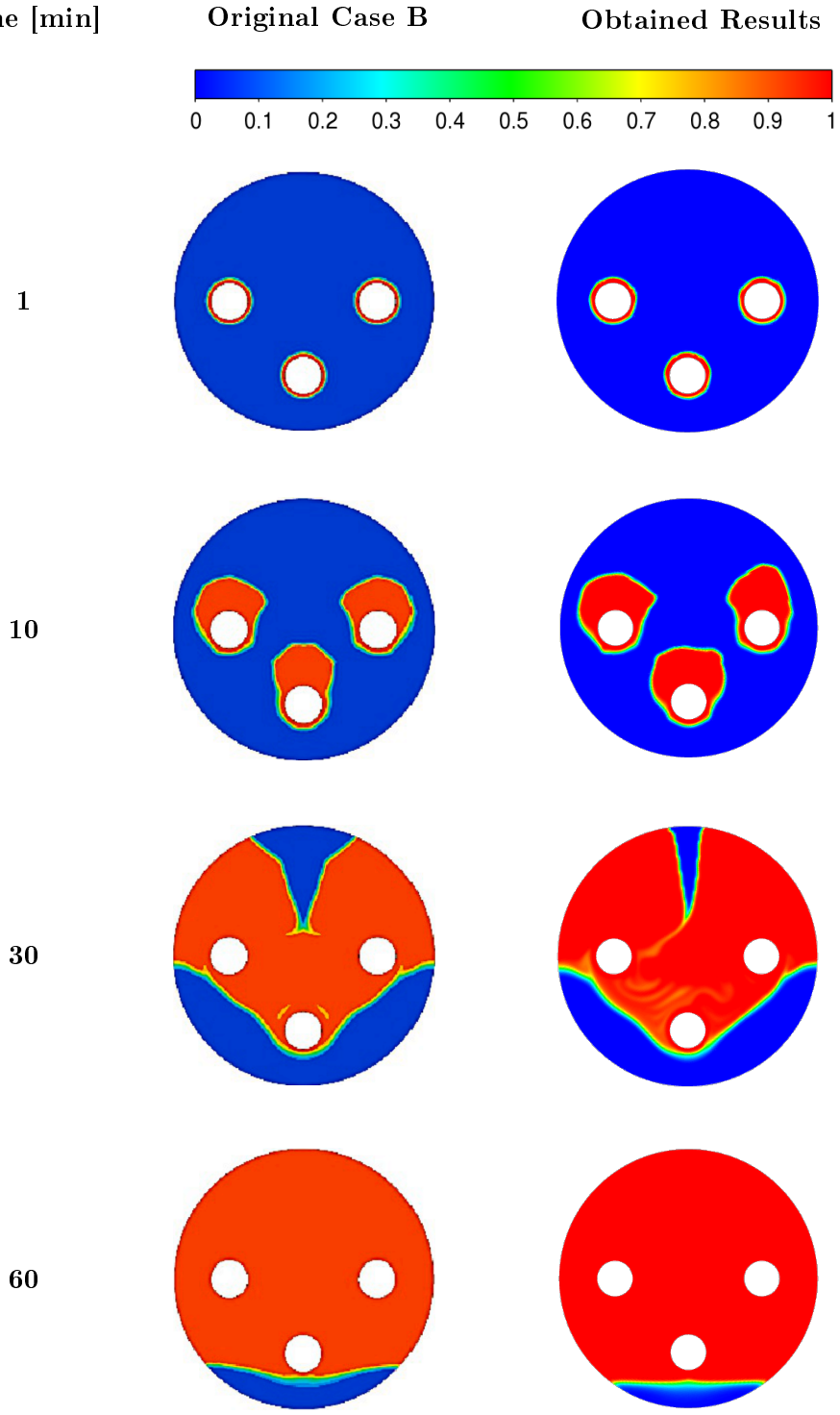

4.4 Strategy Outline

Since the results obtained from the PCM analysis, were compared and validated against the model's original article, the following aim is to improve its application efficiency in similar research. To understand how the processes of energy absorption and release can be more efficient, the available options of influencing factors were analysed.

As described in the beginning of section 3.2 of this document, there are four main factors that influence a PCM application and that can be used as a comparison factor with the previously obtained results. Those are 1) the thermal parameters of the PCM, such as melting temperature or latent heat, or 2) of the HTF used in the application, such as its thermal conductivity or temperature. Also, 3) the incorporation method of the PCM and finally, 4) the configuration of the system in analysis.

For the present case, the use of the incorporation method as an optimization tool is not a viable option, as the validation process of the numerical model would not be applicable to other forms of PCM encapsulations. As to the thermal parameters, the only input given on the numerical model regarding the HTF is the water temperature, as regarding the PCM's, any parameter can be taken into consideration to be a comparison factor.

The article used as a reference was a study of four different cases of HTS arrangements [30]. In this case, the configuration and location of the three pipes in the cross section of the geometry was the issue under consideration, and the comparison between the cases' results is shown in table 4.4. This allowed to draw a conclusion that relates the pipes' configuration, melting rate and the overall melting time of the PCM.

Table 4.4: Results of the four cases of the original article [30]

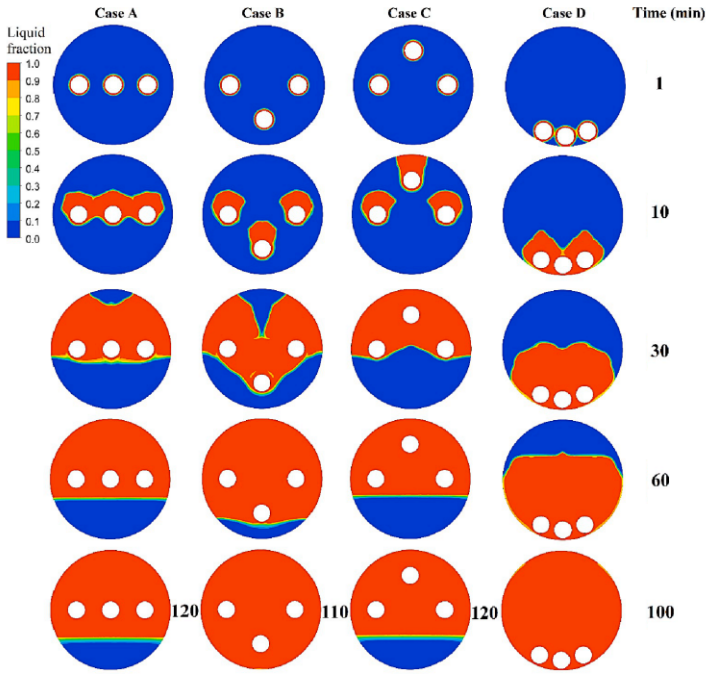

At the start of Mahdi *et al.* experiment [30], the dominant heat transfer mechanism was conduction for all four cases. However, as time progressed, the PCM that was in contact with the HTS began to melt and its density became sufficiently smaller, that by the action of gravity, convection flows were induced. The buoyance force exerted by these hot flows led to a quicker melting of the above regions that are further away from the heat source, rather than the ones below. On all four cases it was clear that due to the above mentioned reasons, the lower the pipes were located in the PCM STHE unit, the quicker the energy absorption process would finish.

To take the most advantage of the findings of the original article, the proposed strategy to optimize the process will also focus on the impact of the induced convection flows on the melting rate. However, instead of studying the influence of the pipes' position inside the STHE unit, the impact of its shape will be addressed.

Chapter 5

Shape Parametric Studies

Knowing beforehand that the horizontality of the HTS is going to affect the rate of the melting process, the proposal to change the shape of the pipes is precisely to evaluate that impact. The pipes' shape and dimensions can be custom ordered and manufactured resorting to extrusion processes to create any desired profile, as the examples of figure 5.1.

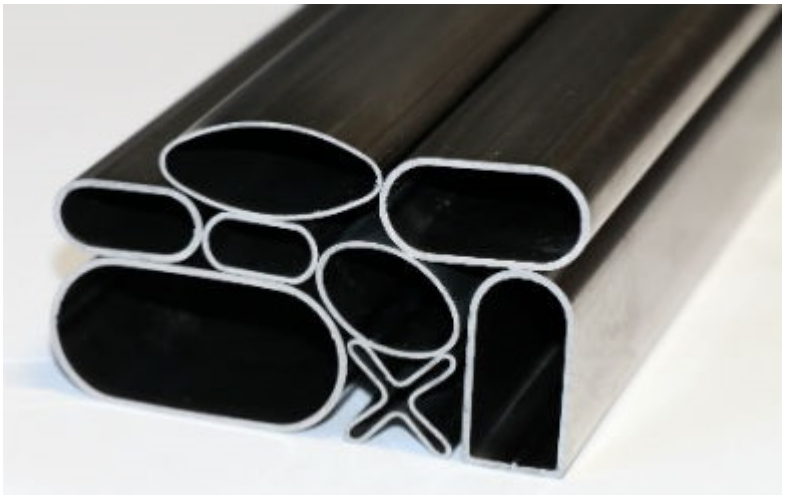

Figure 5.1: Examples of possible pipes profiles

Changing its section from a circle to an ellipse allows the vertical and horizontal dimensions to change, without changing its area and consequentially the flow of the HTF inside the pipe, inferring that way, only, the influence of the different perimeter shape.

5.1 Numerical Definition

5.1.1 Geometry's Description

Considering the initial pipes' radius of $5mm$, the ratio between the ellipse's major and minor axis, a and b respectively, that provides the same area value must be determined according to equation 5.1.

$$A_{circumference} = A_{ellipse} \Rightarrow 5^2\pi = ab\pi \Leftrightarrow a = \frac{25}{b} \tag{5.1}$$

Respecting the above calculated ratio, multiple pairs of values were considered for the ellipse's axis. The values considered for the horizontal axis are equally spaced and consecutively higher on each of the following cases, as shows figure 5.2.

Case 1:

$$\begin{cases} a = 15mm; \\ b = 6.67mm; \end{cases}$$

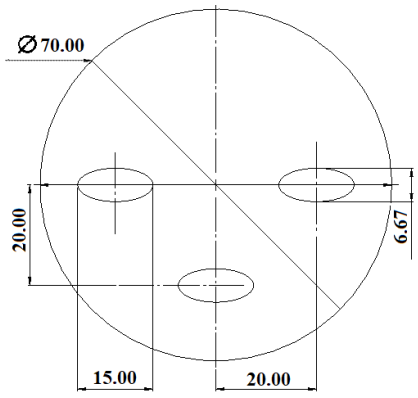

Case 2:

$$\begin{cases} a = 20mm; \\ b = 5mm; \end{cases}$$

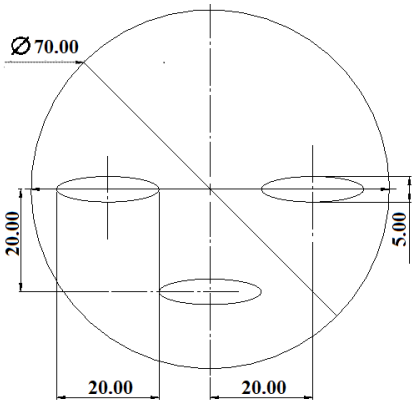

Case 3:

$$\begin{cases} a = 25mm; \\ b = 4mm; \end{cases}$$

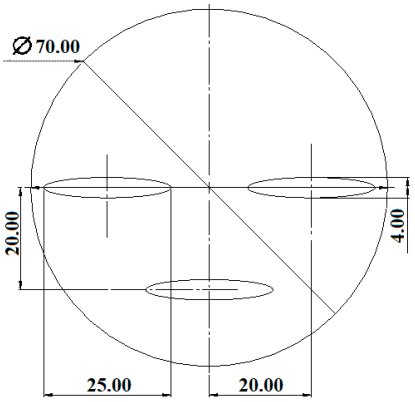

Case 4:

$$\begin{cases} a = 30mm; \\ b = 3.33mm; \end{cases}$$

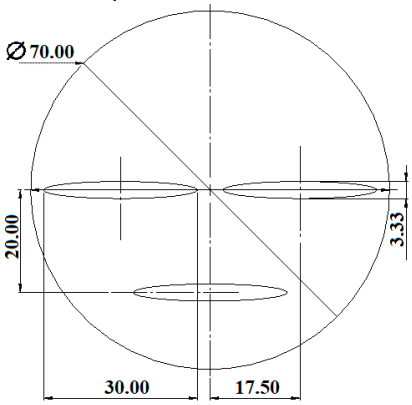

Figure 5.2: Dimensions of each case for analysis

5.1.2 Mesh

Similar to the previous chapter, the geometries presented by the four cases for comparison were also developed on SolidWorks® 2020 software and exported on .igs format file. All four files were then imported to Ansys Fluent®'s meshing module and the same features as the original model were applied on all the cases. A maximum element size of $5mm$ and an inflation layer feature on all three HTS, with a maximum layer number of 20 and a growth rate of 1.5 were used. The final meshes for all cases are presented in figure 5.3.

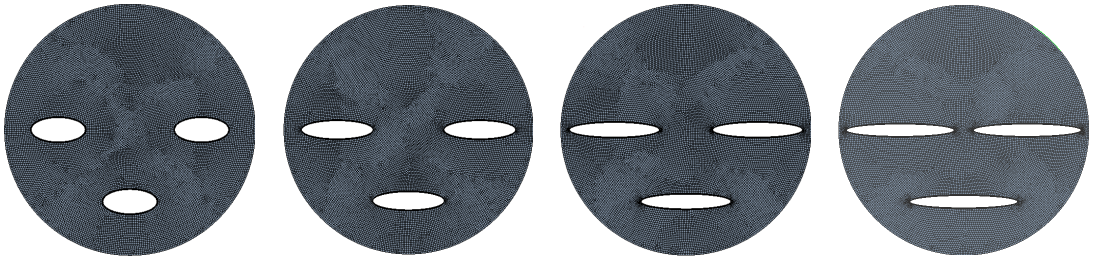

Figure 5.3: Meshes of the cases for analysis

The meshes' quality analysis was performed resorting to two quality control parameters, the orthogonal quality and the skewness. The total number of elements for each case, as well as their percentage that presents mesh quality values considered as very good is shown in table 5.1.

Table 5.1: Total number and percentage of elements of the 4 meshes in the very good quality interval

Mesh Case Number	**Total Number of Elements**	**% of Elements with Orthogonal Quality >0.7**	**% of Elements with Skewness <0.5**
1	18381	89.77%	99.92%
2	20103	86.74%	99.91%
3	22097	81.40%	99.93%
4	24339	80.26%	99.87%

5.1.3 Setup And Solution

The inputs required for Ansys Fluent® setup and solution are the same presented in the model calibration and validation chapter (Chapter 4), given that the analysis case used in the previous chapter was duplicated for each of the following cases. The details regarding setup and solution parameters, such as 1) solver configurations, 2) enabled models, 3) material definitions, iv) boundary conditions, v) methods, vi) controls and vii) residual monitors that were stated from section 4.2.3 to 4.2.6, are still valid.

A change that is worth refering is the adjustment of the HTS boundary condition. Since each case presents a different HTS geometry, the named selection used as scope for this input has to be manually changed, so that the new mesh's edge shape for each case in analysis is considered.

5.2 Results And Discussion

The results of different parameters from the analysed four cases are presented next.

5.2.1 Melting Time

The liquid fraction plots for all cases are displayed in figure 5.4, as well as the original liquid fraction plot for comparisson.

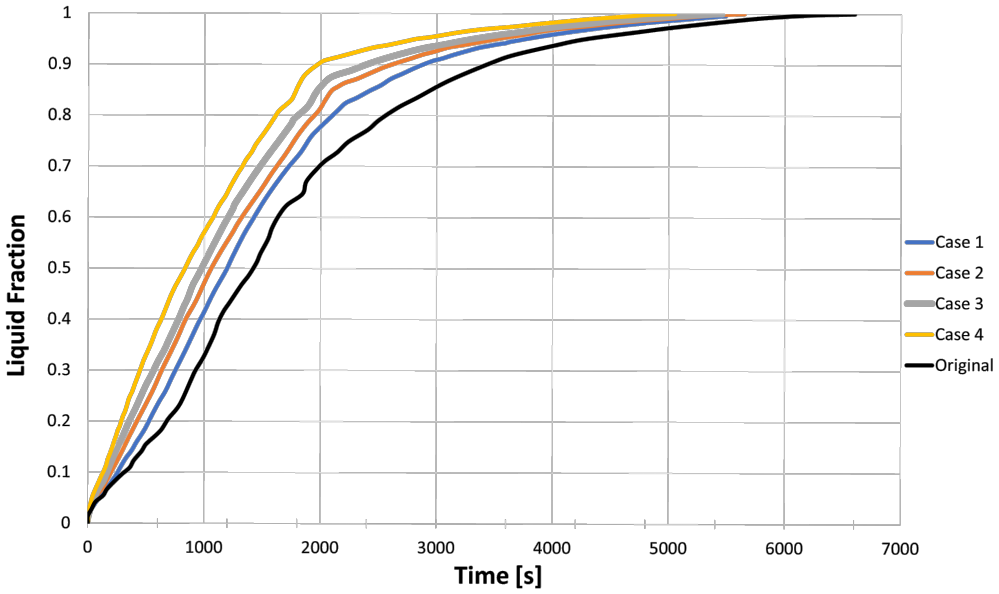

Figure 5.4: Liquid fraction plot for all cases under analysis

The original case presented a total melting time of 110 minutes. As we can observe in table 5.2, the total melting time of case 4 was 5050 seconds which equals 84.17 minutes. This way reducing the total amount of time, to store the same amount of energy, by 25.83 minutes, equivalent to 23.48% of the initial time saved.

To analyse the impact of the different ellipses' shapes in the melting time at which 90% of the volume of PCM has transitioned to liquid phase, the corresponding values for the percentage of time reduced are also shown in table 5.2.

Table 5.2: Melting time values for all cases in analysis

	Total Melting Time [min]	**Time Saved [%]**	**Melting Time to 90% [min]**	**Time Saved to 90% [%]**
Original	110.00	-	57.58	-
Case 1	97.48	11.38	48.71	15.40
Case 2	94.17	14.39	44.22	23.20
Case 3	90.96	17.30	39.90	30.71
Case 4	84.17	**23.48**	36.16	**37.20**

The behaviour observed during the last stages of the simulation, after roughly the 90% of liquid fraction value has been reached, is that the last 10% take in average 47.3% of the total simulation time to reach full volume liquid phase stage.

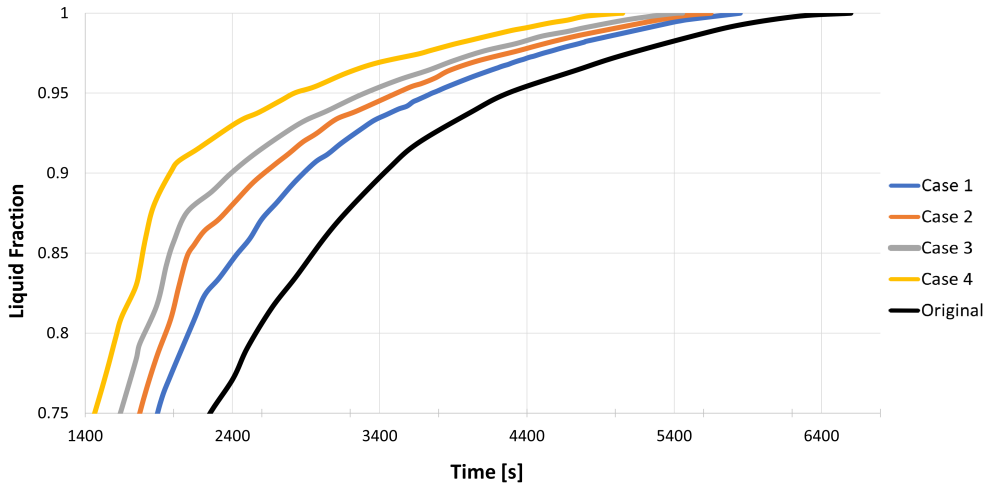

Figure 5.5: Over 90% liquid fraction plot for the four cases under analysis

This is justified by the energy transfer rate value between the material and the fluid, being dependent on the temperature difference between the two, which keeps decreasing during the simulation.

This is similar to other types of energy storages systems like electric batteries, in which charging rate decreases as the batteries' storage increases. Also, the lack of influence of the convection flows on the solid volume of material, results on a longer period of time for the remaining volume to melt.

5.2.2 Melting Rate

Analysing the liquid fraction results, their slope suggests that the melting rate of the PCM increased with the horizontality of the HTS, as initially predicted. However, further analysis evaluated their individual slope values.

Due to the significant variation of the results slope before and after the 2000 seconds mark, time around which the volume of PCM above the HTS has melted entirely, this analysis was divided in two time intervals, so that the two slopes can be determined for each case.

The first melting slope, calculated in table 5.3, refers to the first 2000 seconds (33.33 min) of simulation and the second melting slope considers the remaining simulation time.

Table 5.3: Slope values for the liquid fraction graphs of cases under analysis

	Time Δx_1 **[min]**	**Liquid Fraction** Δy_1 **-**	**First Melting Slope** $\Delta y_1/\Delta x_1$ **[min^{-1}]**	**Time** Δx_2 **[min]**	**Liquid Fraction** Δy_2 **-**	**Second Melting Slope** $\Delta y_2/\Delta x_2$ **[min^{-1}]**
Original	33.33	0.7023	2.11E-02	76.67	0.2977	3.88E-03
Case 4	33.33	0.7777	2.33E-02	64.15	0.2223	3.47E-03
Case 3	33.33	0.8157	2.45E-02	60.84	0.1843	3.03E-03
Case 2	33.33	0.8566	2.57E-02	57.63	0.1434	2.49E-03
Case 1	33.33	0.9033	2.71E-02	50.84	0.0967	1.90E-03

As expected from the visual observations of the liquid fraction plots, the values for the first melting slope increase along with the HTS perimeter, however the values for the slope of the melting rate after 33 minutes of simulation decreases instead. To have a better understanding of the real variation when comparing multiple cases, a tree diagram for each of the melting slope intervals considered summarizes the percentages of slope increase, on the left, as well as decrease, on the right.

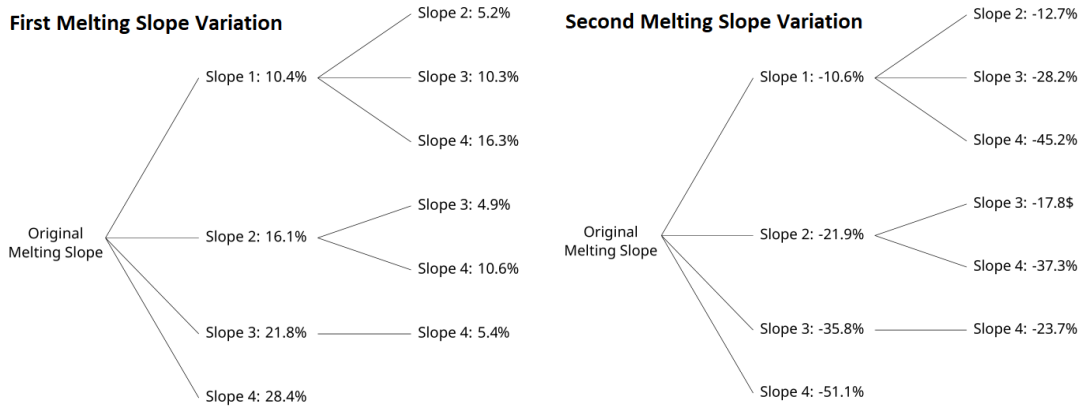

Figure 5.6: Percentage of variation in slope values for each case; Left: First interval melting slope variation; Right: Second interval melting slope variation

For the first time range considered, case 4 presents the highest improvement in the melting rate of the volume of PCM, with a value 28,4% higher than the original case. It is also possible to infer that, with the exception of the first case, each of the following cases presents an increase of approximately 5% in its melting rate, when compared to the previous case.

For the second time range, it is found that the original case presents a slope value more than twice the value of the one of case 4. However, at the instant in which the considered interval begins, case 4 presents a liquid fraction value that is 28.5% higher than the original case's, the lower slope in this time range still allows for case four to be the one in the most developed stage when comparing all the cases under analysis.

5.2.3 Liquid Fraction

To analyse how these different stages of development influence the progress of the simulation in more detail, liquid fraction values were determined. The liquid fraction values vary between 0 and 1, according to the percentage of the considered volume of PCM that has transitioned from the solid to the liquid state, and they are presented and compared in table 5.4.

Table 5.4: Liquid fraction values for all cases under analyis

	Time [min]								
	1	**10**	**20**	**30**	**40**	**50**	**60**	**70**	**80**
Original	0.034	0.203	0.428	0.661	0.771	0.856	0.914	0.947	0.966
Case 1	0.038	0.259	0.504	0.720	0.846	0.908	0.943	0.966	0.982
Case 2	0.046	0.281	0.556	0.758	0.881	0.9203	0.953	0.973	0.987
Case 3	0.055	0.318	0.600	0.802	0.901	0.937	0.961	0.978	0.991
Case 4	0.065	0.384	0.649	0.855	0.928	0.954	0.973	0.987	0.998

Due to the density of results, and in order to visualize their meaning more clearly, two graphs were created based on the previously obtained data. The increase percentage in the liquid fraction values for each time for all cases was calculated.

i) Cases to original Shown in figure 5.7, the increase percentage of each value in relation to the corresponding value of the original case. We can clearly observe how each consecutive case presents a more developed stage of the phase change process for the same time.

The explanation for this, considering minute 10 of table 5.5, is that the horizontal reach of the convection flows induced is much larger and consequentially so is the volume of PCM that is influenced by them.

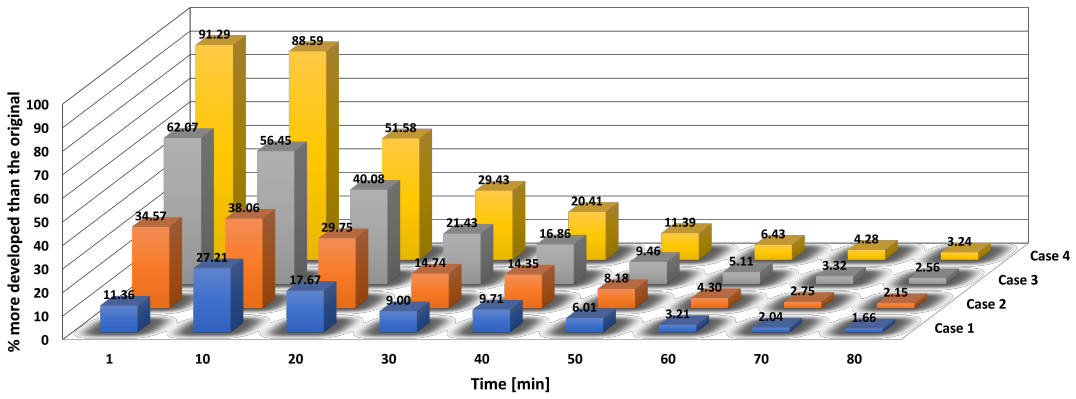

Figure 5.7: Percentage of improvement of each case in relation to the original case

However, the impact of the shape is also less significant as time progresses in the melting process for all the cases in analysis. This can be explained by the lack of solid volume of PCM above the HTS after the 30 min mark, since the induced convection flows will no longer have the same impact in the melting process. This is consistent with the drastic decrease of the melting rates for all cases shown in figure 5.4.

ii) Cases to previous Shown in figure 5.8, the increase percentage of each value in relation to the corresponding value of the previous case. Here we can observe that the difference from the original case to case 1, with the introduction of the ellipse, is more significant than the improvement between any other cases on all time references except the first minute.

This lack of a similar impact in the first minute can be explained by the fact that conduction is the predominant heat transfer phenomenon in the begining of the melting process. The latest cases present a higher HTS perimeter, so the influence of that value will be bigger than the convection flows induced at an early time.

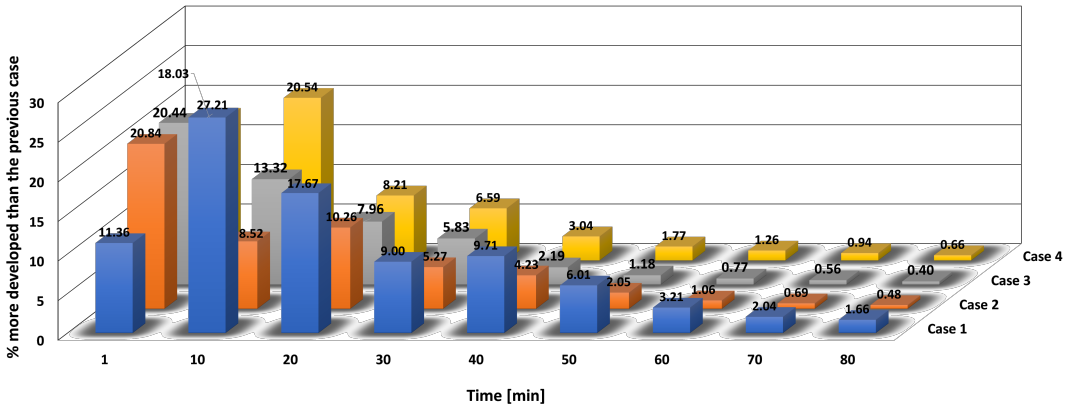

Figure 5.8: % of improvement of each case in relation to the previous case

Table 5.5 presents the liquid fraction countours for the proposed four cases proposed, with a elliptic HTS shape, for the above mentioned reference times. Observing the contours of the first minute of simulation, the PCM begins to melt around the perimeter of the pipes as expected, however, not even the difference in size of the perimeter or its horizontality, is relevant enough to observe any convection induced melting.

On the contrary, in the minute 10, is clear the impact of the horizontal reach in case 4, presenting as evaluated in table 5.4 a liquid fraction value almost 50% higher than case 1. For minute 20, case 4 presents the highest liquid fraction of 30% more, however, this difference in the values between the two extreme cases decreases consecutively from minutes 30 to 50, as shown in table 5.7.

Table 5.5: Liquid fraction contours for the four cases in analyis

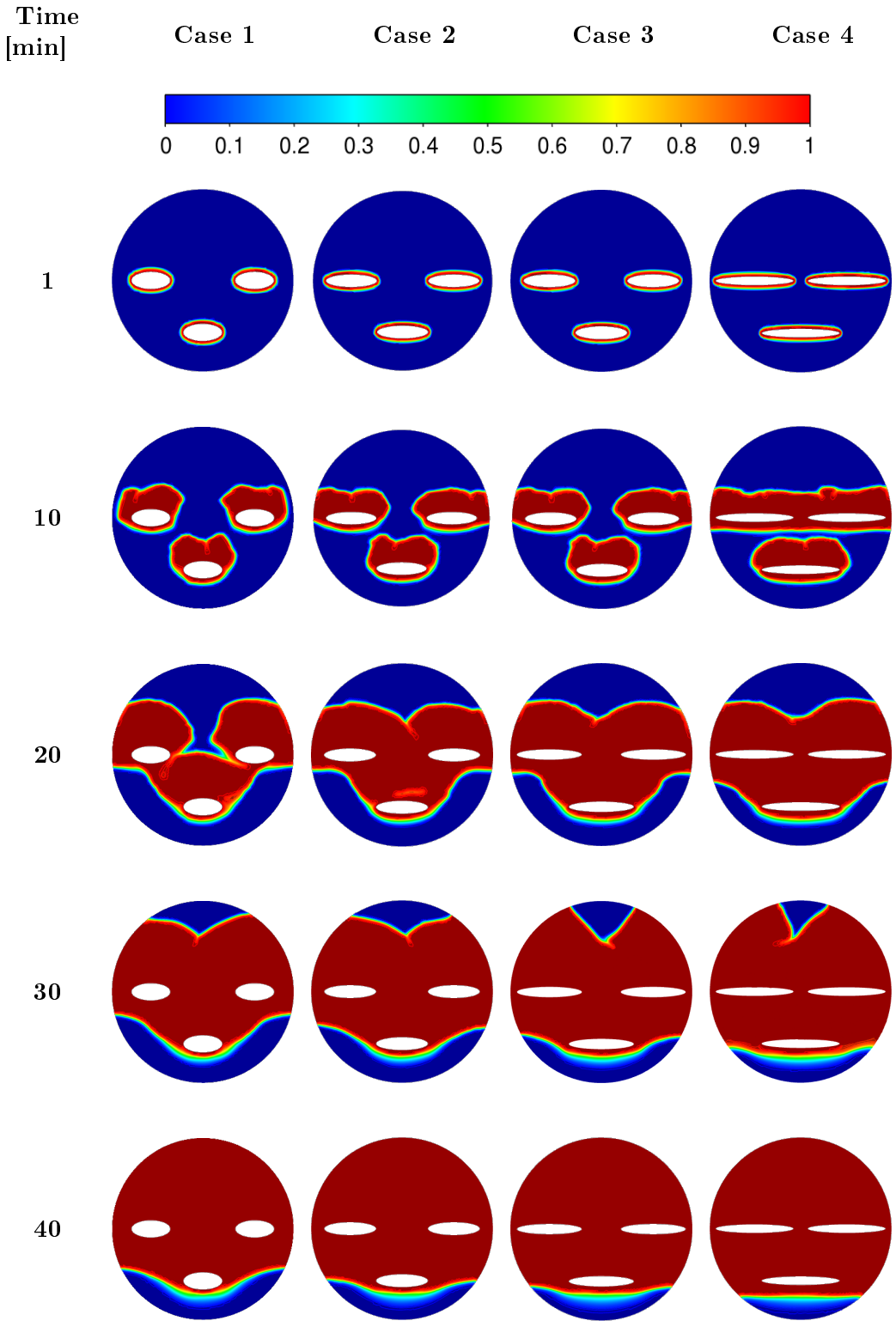

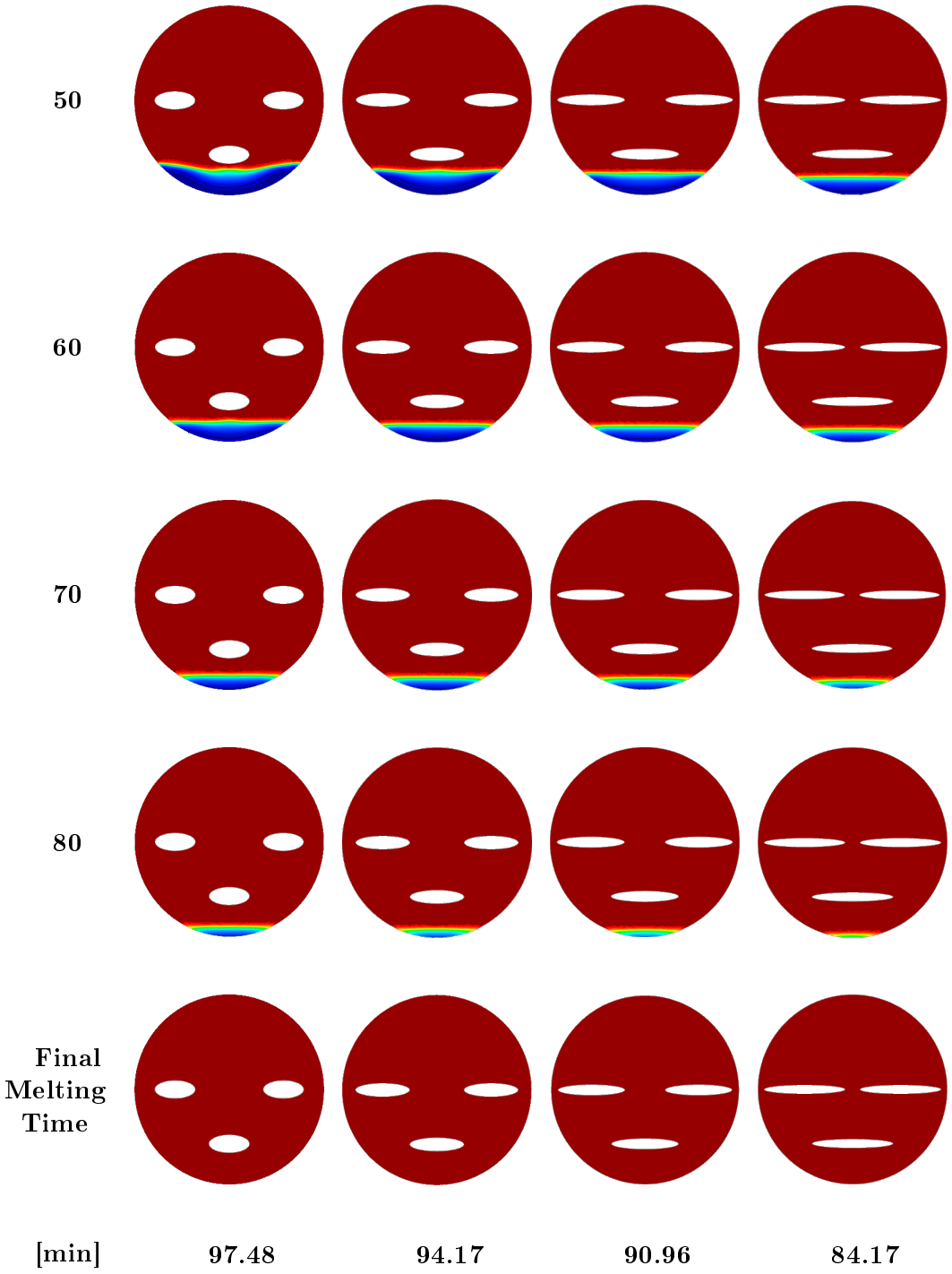
50
60
70
80
Final Melting Time
[min]
97.48
94.17
90.96
84.17

5.2.4 Heat Transfer

Regarding the fluxes through existing boundaries, and to understand the impact of the perimeter of the ellipse in the heat transfer to the system, the heat transfer values for the first seconds of the simulation were also extracted for all cases. Even though the comparison with the original case is not possible due to the absence of values, an assessment of the improvement between the proposed cases is still relevant.

The graph of these values for the first 60 seconds is displayed in figure 5.9. After this instant, the difference in the slope and values for the four cases is neglectable.

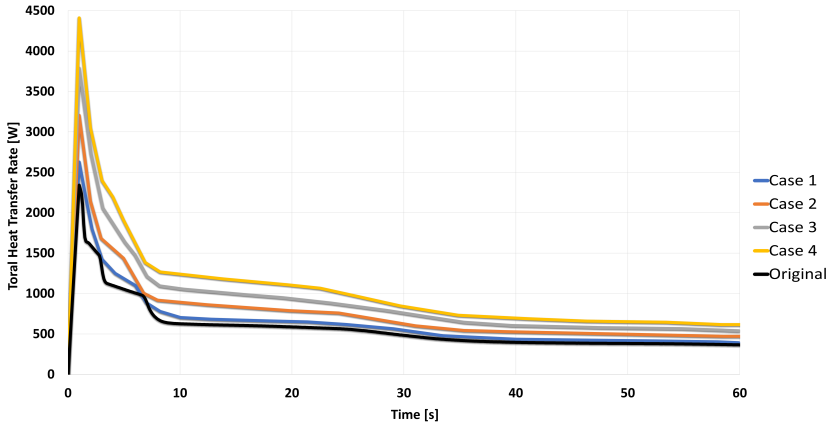

Figure 5.9: Heat transfer rate graph for the first 60 seconds

The corresponding peak values of each case of figure 5.9 are shown in table 5.6. The outcome of this results confirms the expected tendency for the total heat transfer rate to rise along with the increased perimeter.

Table 5.6: Peak values of heat transfer rate for each case in analysis at 1s

	Total Heat Transfer [W]	**Variation [%]**
Original	2341.64	-
Case 1	2635.84	12.56
Case 2	3228.08	37.86
Case 3	3785.43	61.66
Case 4	4430.31	89.20

Furthermore, case 4 presents a value 68.1% higher than case 1 and 89.1% higher than the original case. However, this value is not very significant in a long term analysis, since the temperature difference between both sides of the HTS rapidly decreases with the melting of the PCM on its periphery. Due to this temperature balance in both sides of the transfer area, the heat transfer rate stabilizes at a much lower value after the 60 seconds.

5.2.5 Convection Velocity

To address the impact of the HTS shape in the velocity of the convection flows, the average velocity of the whole volume of PCM was evaluated. Figure 5.10 presents the values of average velocity for all cases during the first 200 seconds of simulation. Due to the lack of horizontality and less contact area on the original case, the heat transfer happens by conduction through the HTS to a smaller volume than the conduction of case 4. This concentrated conduction leads to a higher velocity magnitude of the PCM around the circular edge, as shows the left velocity contour of figure 5.11.

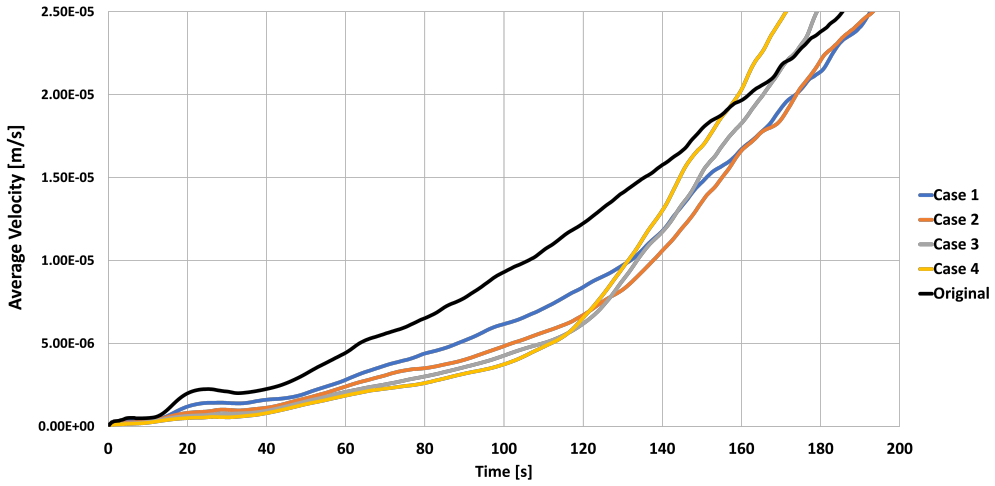

Figure 5.10: PCM average velocity values for all cases in analysis

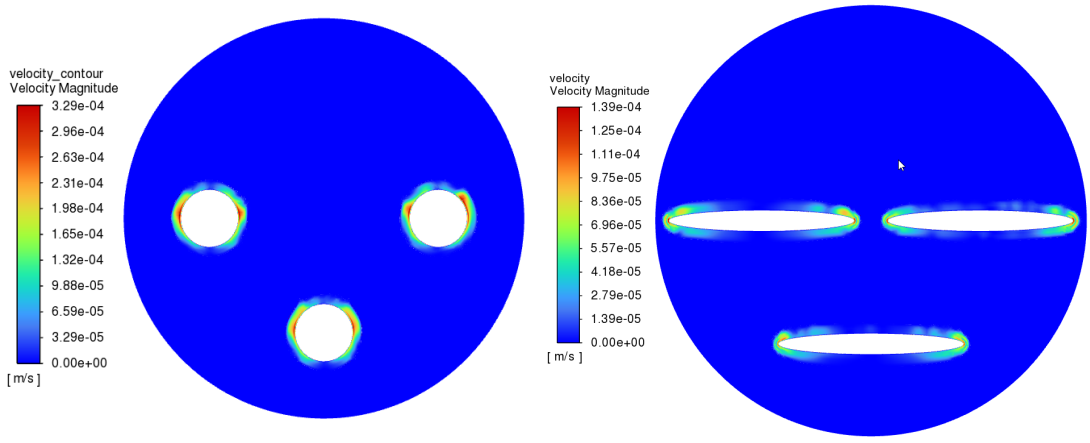

Figure 5.11: Average velocity contours for original case (left) and case 4 (right)

The peak of high velocity values in the circular HTS during the initial seconds becomes less relevant as its sorroundings continue to melt on all cases. Around the 120 seconds, figure 5.10 shows the slope of all cases inverting, with the horizontality increase presenting higher velocity values. Tendency which is mantained for the following 1500 seconds of the simulation time, as shows figure 5.12.

As already approached, case 4 reveals a more developed melting rate than the other cases, this also results in a sooner peak of average velocity values. As figure 5.12 shows, the more horizontal the shapes are the lowest values of velocity they present, except for the original case which presents a peak value more than 50% lower than the average of the other four, as shows table 5.7.

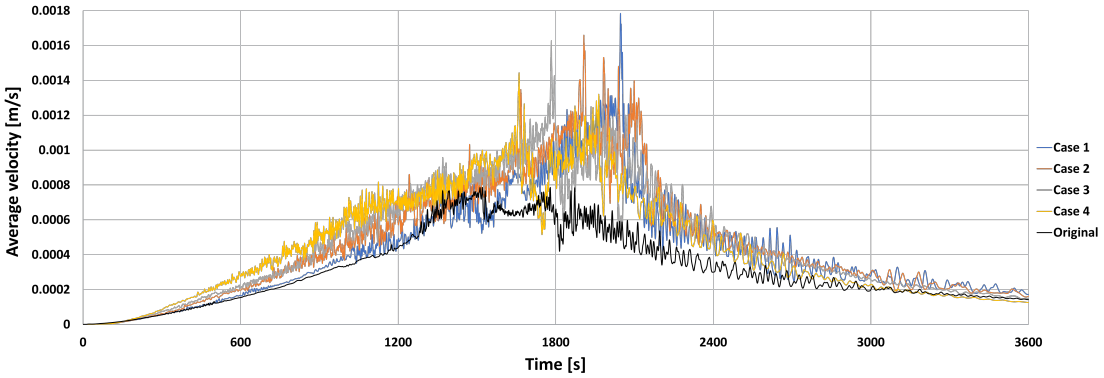

Figure 5.12: PCM average velocity values for all cases in analysis

Until it reaches its peak, case 4 presents the higher average of velocity values when comparing with all the other cases. Once case 4 values start decreasing, the highest average values are case 3, until case 3 also reaches its peak, and the same trajectory is followed by the remaining two cases. However, the peak values are increasingly higher with a smaller ellipse, as shows table 5.7, that compiles the maximum values for each case and their corresponding times. Also shown in the same table is that each 5 mm increase in the horizontality of the HTS, results in approximately 7% of time saved to achieve the velocity peak.

Table 5.7: Peak values and respective times for PCM average velocity

	Peak value of average velocity [m/s]	**Time of peak value of average velocity [min]**	**Time of peak variation [%]**
Original	7.86e-4	25.35	-
Case 4	1.44e-3	27.68	9.14398
Case 3	1.63e-3	29.73	7.40607%
Case 2	1.66e-3	31.79	6.92903%
Case 1	1.78e-3	34.11	7.29789%

After 40 minutes the values of the four proposed cases decrease at similar rates and with similar velocity values, which is consistent with the liquid fraction contours observed in table 5.5, that also showed the volume of PCM above the HTS had melted entirely at this stage. After 60 minutes the difference in the cases' velocity values are neglectable.

5.2.6 Temperature

The average temperature values of the overall volume of PCM is shown in figure 5.13 for each cases. The results show that the values of average temperature are very similar in all cases. However, we can observe that the time it is required to achieve them, varies with the horizontality of the HTS shape. Case 4 presents the case in which the temperature increases faster, which is consistent with the higher melting rate and convection velocity values analysed previously.

The graphs also show a steep decrease in temperature at around half of the analysis time. The time during which this happens is consistent with the transition between the first and second melting slopes, described in the melting rate analysis.

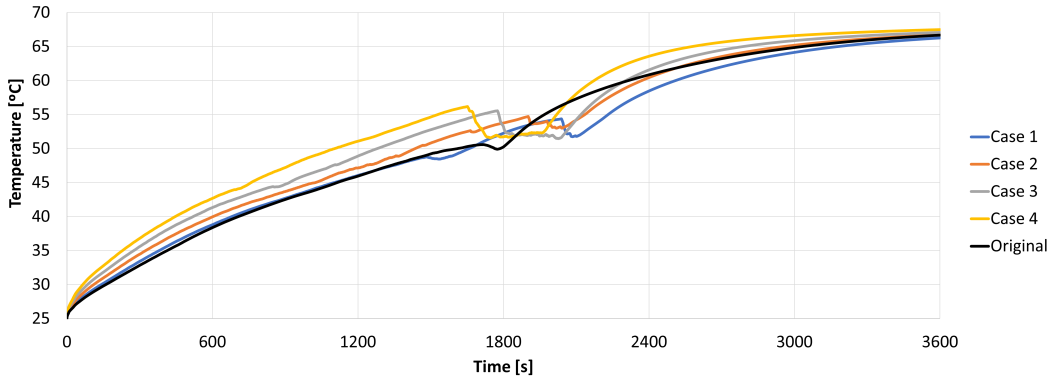

Figure 5.13: Average temperature values for all cases in analysis

The temperature contours of the PCM are shown in table 5.8. In the first minute, it is noticeable the higher temperatures concentrating around case 4 HTS rather than case 1. This tendency is mantained until the surrounding area reaches a similar temperature to the pipes' edges.

From the 10 minutes until the 40 minutes, its possible and easy to distinguish the induced convection flows that are formed in the volume of material, due to the temperature difference that enables the convection movement. This highlights a clear tendency for case 1 to develop merely one hotspot near the center of the ellipse's top semi-arch, that then progresses into one convection flow. However, when comparing to any of the other cases, their ellipses present two or more hotspots on their top semi-arch, leading to multiple convection flows arising from each HTS.

On the 10 minutes contours, the main differences between the two extreme cases is both the temperature of the induced flows, as well as the volume of PCM which has been influenced by them. From 20 to 40 minutes however, the volume present an affected area that is quite similar in all cases, but it also displays an even higher overall PCM temperature difference between cases 1 and 4.

The 40 minutes is the last time reference in which a significant temperature difference still exists between the cases under analysis. This mitigation and standardization is also consistent with the lack of solid PCM above the HTS after this period.

Table 5.8: Temperature contours for the four cases

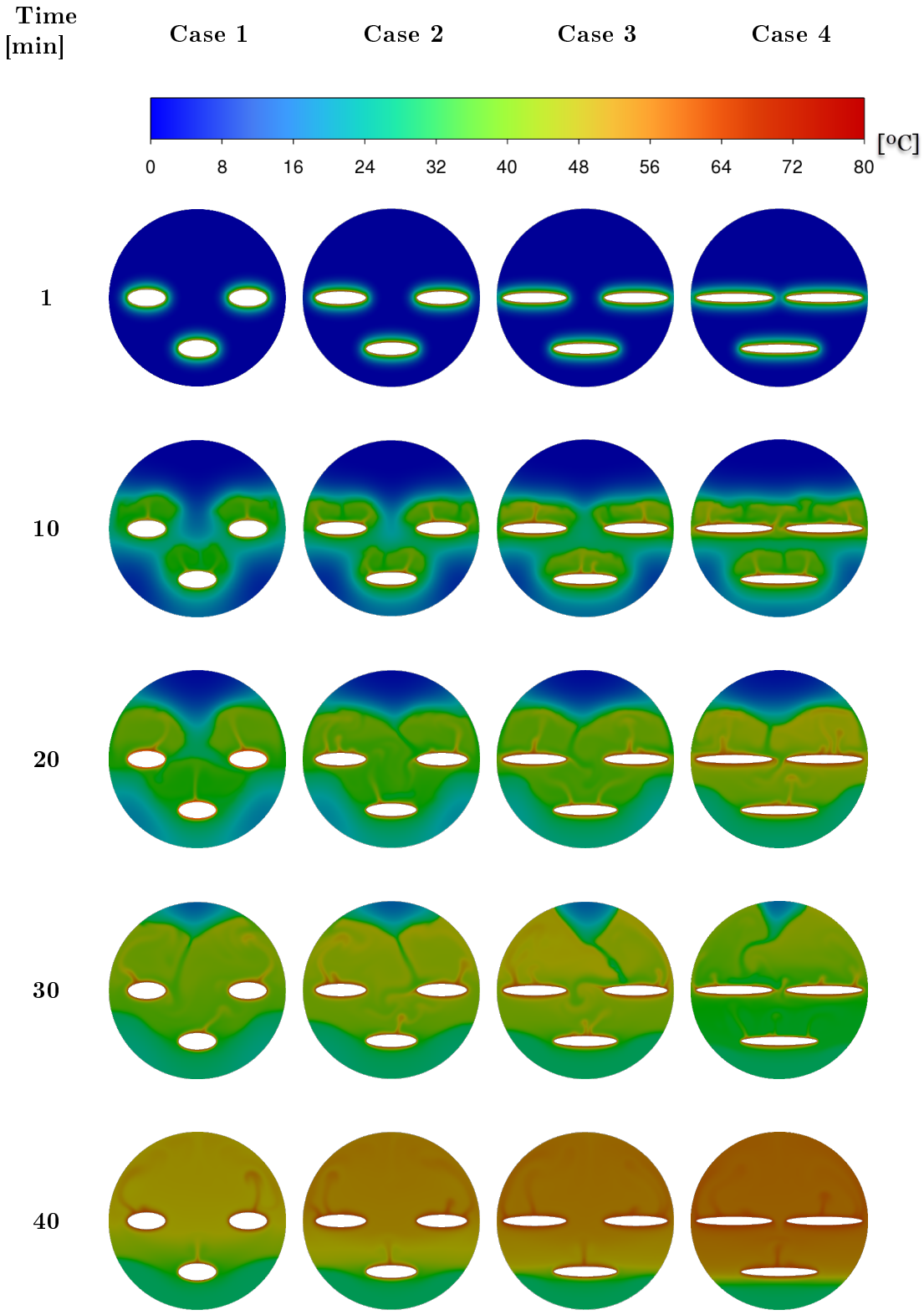

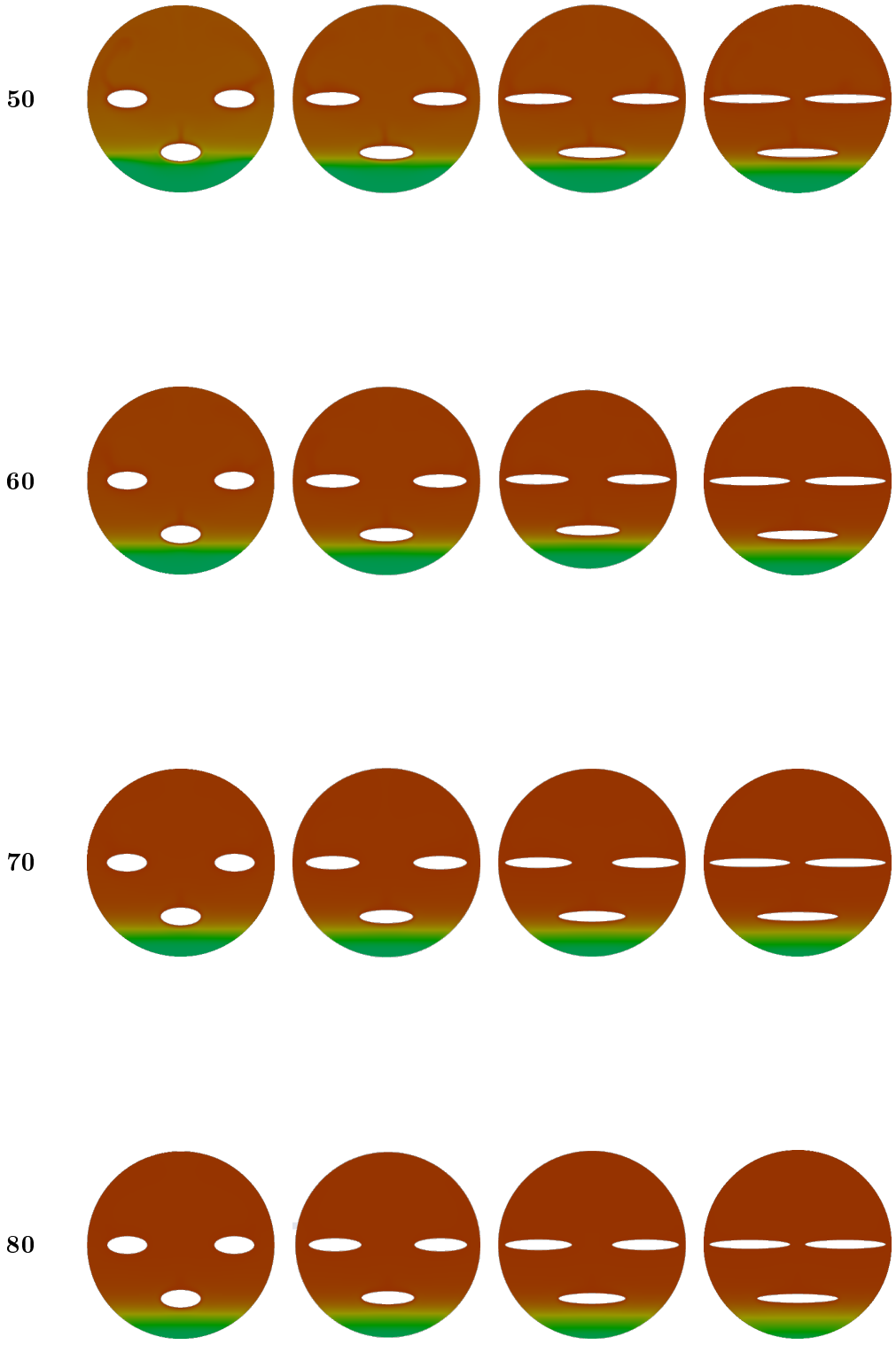
50
60
70
80

Chapter 6

Conclusions

The initial goal was to present a strategy that could improve the efficency of household's heating systems, by allowing free and cheap energy to be stored in thermal energy systems until required for use. This study numerically investigated the impact of the cross section shape of a STHE pipe on a 2D CFD model. Four parametric cases were developed to evaluate the findings and assess the influence of the HTS's horizontality on the temperature distribution that affects the induced convection flows, and consequentially the PCM charging time.

After analysing the results obtained from the proposed strategy, its confirmed that the horizontal component registers a better performance in all the parameters evaluated. These elongated shapes display a bigger perimeter, which in turn leads to a higher peak of heat transfer from the HTF to the PCM in the first instants.

However, their effect lasts in time, since a more horizontal surface creates more hotspots on its edges than a circular one, that then leads to a higher number of convection flows, affecting more volume per unit of time. But not only does it present more convection flows, horizontal shapes also mantain a higher average of convection velocity.

The best performing option allowed for a charging time reduction of 23.48% comparing to the original case. A reduction of the total time of simulation as the one obtained, means that any source of electricity that is providing the off-peak energy to store, will require approximately three fourths of the time it did with the original solution adopted, and consequentially decrease the chargind cost accordingly.

When considering the possibility of coupling PCM based energy storage systems with renewable energy capture methods, such as solar water systems, the energy rate between the heated water and the PCM is crucial for the overall readiness of the system, since these sources' presence and intensity are unstable and unpredictabble. The presented solution also allowed the system to charge 90% of total capacity in 37.2% less of the time of the original system, meaning that the same performance will be achieved in days with only 62.8% of the previously required solar exposure.

From case 1 to case 4, it was also noticeable the increase of 68.1% in the heat transfer rate peak values, justified by an HTS perimeter almost double the size of the first case's ellipse.

In short, each 5 mm increase on the HTS horizontal reach, resulted in an average of i) 9% of simulation time saved to reach the 90% liquid fraction, ii) 5% increase in the first stage melting rate of the PCM, iii) 20% increase of the heat transfer peak values and finally, iv) 7% of time reduction to hit convection velocity peak values.

After a reflexion on the initial study case of the original article that was chosen, it is clearer now that the vertical positioning of the middle ellipse was not given sufficient importance in the strategy later developed. This reflected itself when the melting rates of all four cases decreased drastically once the volume of PCM above the HTS in solid state was null.

One of the most impactful limitations faced in the development of this study, is the extensive computational time required to simulate each one of the developed cases. Other limitations in the accuracy of the final results arise from the solver's simplifications and considerations, such as the adopted boussinesq approximation that assumes that density is considered constant in all its equation terms except when associated with the gravity variable, which allows for the natural convection phenomenon to be considered and recognizable. However this introduces other constraints, since all other thermal parameter values are considered constant and not temperature dependent, neglecting the effect of possible viscous dissipation, as investigated by Mulamootil *et al.* [42].

For future work, to decrease the charging time of the PCM even more, the last 10% of material to melt who represents over 40% of the overall time, can be tackled. A lesson learned was that the influence of the middle HTS would have been significantly higher in decreasing this melting time, if located in an even lower position near the outside tube's edge. This way the induced convectin flows would have an influence in the melting process for a longer period of time, and the melting rate wouldn't decrease as drastically so soon.

———————————————————————————-

Bibliography

[1] Vaclav Smil. Energy - Our World in Data, 2017.

[2] Eurostat Statistics Explained. Final energy consumption by sector, EU-28, 2017.

[3] Ricardo da Cunha Norte Mendes. Materiais de mudança de fase para aquecimento em escoamentos laminares. Technical report, 2013.

[4] Harald Mehling; Luisa F. Cabeza. *Heat and cold storage with PCM*, volume 11. 2000.

[5] Hassan Nazir, Mariah Batool, Francisco J. Bolivar Osorio, Marllory Isaza-Ruiz, Xinhai Xu, K. Vignarooban, Patrick Phelan, Inamuddin, and Arunachala M. Kannan. Recent developments in phase change materials for energy storage applications: A review. *International Journal of Heat and Mass Transfer*, 129:491–523, 2019.

[6] D. Zhou, C. Y. Zhao, and Y. Tian. Review on thermal energy storage with phase change materials (PCMs) in building applications. *Applied Energy*, 92:593–605, 2012.

[7] Pedro Miguel and Baptista Teixeira. Materiais de mudança de fase em processos de aquecimento: propriedades. Technical report, 2013.

[8] Ardeshir Mahdavi. Phase Change Materials as Variable Heat Storage in the Built Environment. (November), 2020.

[9] Yalin Zhu, Yaosong Qin, Chengsha Wei, Shuen Liang, Xuan Luo, Jianhua Wang, and Lin Zhang. Nanoencapsulated phase change materials with polymer-SiO2 hybrid shell materials: Compositions, morphologies, and properties. *Energy Conversion and Management*, 164(February):83–92, 2018.

[10] A. Mavrigiannaki and E. Ampatzi. Latent heat storage in building elements: A systematic review on properties and contextual performance factors. *Renewable and Sustainable Energy Reviews*, 60:852–866, 2016.

[11] A. Abhat. Low temperature latent heat thermal energy storage: Heat storage materials. *Solar Energy*, 30(4):313–332, 1983.

[12] A. S. Hariri and I. C. Ward. A review of thermal storage systems used in building applications. *Building and Environment*, 23(1):1–10, 1988.

[13] Tian Yan, Ji Li, Jiajia Gao, Xinhua Xu, and Jinghua Yu. Model validation and application of the coupled system of pipe-encapsulated PCM wall and nocturnal sky radiator. *Applied Thermal Engineering*, 194(December 2020), 2021.

[14] Hamza Faraji, Ayman Benkaddour, Kenza Oudaoui, Mustapha El Alami, and Mustapha Faraji. Emerging applications of phase change materials: A concise review of recent advances. *Heat Transfer*, 50(2):1443–1493, 2021.

[15] Hang Yu, Chaoen Li, Kege Zhang, Yin Tang, Yuan Song, and Meng Wang. Preparation and thermophysical performance of diatomite-based composite PCM wallboard for thermal energy storage in buildings. *Journal of Building Engineering*, 32(August):101753, 2020.

[16] Tiago Manuel Rodrigues Silva. *Análise numérica e experimental para o desenvovimento de uma proteção solar com incorporação de materiais de mudança de fase.* PhD thesis, 2016.

[17] Steinar Grynning, Francesco Goia, Egil Rognvik, and Berit Time. Possibilities for characterization of a PCM window system using large scale measurements. *International Journal of Sustainable Built Environment*, 2(1):56–64, 2013.

[18] Eman Bellah S. Mettawee and Ghazy M.R. Assassa. Experimental study of a compact PCM solar collector. *Energy*, 31(14):2958–2968, 2006.

[19] J. F. Belmonte, P. Eguía, A. E. Molina, and J. A. Almendros-Ibáñez. Thermal simulation and system optimization of a chilled ceiling coupled with a floor containing a phase change material (PCM). *Sustainable Cities and Society*, 14(1):154–170, 2015.

[20] Kailiang Huang, Guohui Feng, and Jianshun Zhang. Experimental and numerical study on phase change material floor in solar water heating system with a new design. *Solar Energy*, 105:126–138, 2014.

[21] M. M. Farid and X. D. Chen. Domestic electrical space heating with heat storage. *Proceedings of the Institution of Mechanical Engineers, Part A: Journal of Power and Energy*, 213(2):83–92, 1999.

[22] M. Farid and W. J. Kong. Underfloor heating with latent heat storage. *Proceedings of the Institution of Mechanical Engineers, Part A: Journal of Power and Energy*, 215(5):601–609, 2001.

[23] Kunping Lin, Yinping Zhang, Xu Xu, Hongfa Di, Rui Yang, and Penghua Qin. Experimental study of under-floor electric heating system with shape-stabilized PCM plates. *Energy and Buildings*, 37(3):215–220, 2005.

[24] Kunping Lin, Yinping Zhang, Xu Xu, Hongfa Di, Rui Yang, and Penghua Qin. Modeling and simulation of under-floor electric heating system with shape-stabilized PCM plates. *Building and Environment*, 39(12):1427–1434, 2004.

[25] Kunping Lin, Yinping Zhang, Hongfa Di, and Rui Yang. Study of an electrical heating system with ductless air supply and shape-stabilized PCM for thermal storage. *Energy Conversion and Management*, 48(7):2016–2024, 2007.

[26] Isabel Cerón, Javier Neila, and Mohamed Khayet. Experimental tile with phase change materials (PCM) for building use. 43:1869–1874, 2011.

[27] Xing Jin and Xiaosong Zhang. Thermal analysis of a double layer phase change material floor. *Applied Thermal Engineering*, 31(10):1576–1581, 2011.

[28] Yi Xia and Xiao Song Zhang. Experimental research on a double-layer radiant floor system with phase change material under heating mode. *Applied Thermal Engineering*, 96:600–606, 2016.

[29] D. L. Zheng, L. J. Yu, and H. W. Tan. Design and optimization of zero-energy-consumption based solar energy residential building systems. *IOP Conference Series: Earth and Environmental Science*, 93(1), 2017.

[30] Mustafa S. Mahdi, Hameed B. Mahood, Ahmed A. Alammar, and Anees A. Khadom. Numerical investigation of PCM melting using different tube configurations in a shell and tube latent heat thermal storage unit. *Thermal Science and Engineering Progress*, 25(July), 2021.

[31] Ansys User Guide. ANSYS FLUENT 12.0 User's Guide.

[32] Ansys User Guide. Ansys Setup Procedure for Solidification and Melting models.

[33] MechanicalLand. Orthogonal Quality in Ansys Meshing.

[34] MechanicalLand. Looking To Element Quality In ANSYS Meshing.

[35] MechanicalLand. Skewness of Mesh Structures in Ansys Meshing.

[36] N. Fatchurrohman and S. T. Chia. Performance of hybrid nano-micro reinforced mg metal matrix composites brake calliper: Simulation approach. *IOP Conference Series: Materials Science and Engineering*, 257(1), 2017.

[37] Mathura Kumar and D. Jaya Krishna. Influence of Mushy Zone Constant on Thermohydraulics of a PCM. *Energy Procedia*, 109(November 2016):314–321, 2017.

[38] Mohamed Fadl and Philip C. Eames. Numerical investigation of the influence of mushy zone parameter Amush on heat transfer characteristics in vertically and horizontally oriented thermal energy storage systems. *Applied Thermal Engineering*, 151(November 2018):90–99, 2019.

[39] Ansys User Guide. Natural Convection and Buoyancy-Driven Flows.

[40] Automeris. WebPlotDigitizer.

[41] J. Cipriano, G. Mor, D. Chemisana, D. Pérez, G. Gamboa, and X. Cipriano. Evaluation of a multi-stage guided search approach for the calibration of building energy simulation models. *Energy and Buildings*, 87:370–385, 2015.

[42] Jacob Koshy Mulamootil and Sukanta Kumar Dash. Augmentation and diminution of non-Boussinesq effects due to non-Newtonian power-law behavior in natural convection. *International Journal of Thermal Sciences*, 151(January), 2020.